DISSERTATION

The Importance of the periosteum and the induced membrane for bone healing

Die Bedeutung des Periosts und der induzierten Membran für die Knochenheilung

zur Erlangung des akademischen Grades
Doctor medicinae (Dr. med.)

vorgelegt der Medizinischen Fakultät

Charité – Universitätsmedizin Berlin

von

Anselm B. C. Rommel

Erstbetreuer*in: PD Dr. med. Sven Märdian

Datum der Promotion: 30.11.2023

Table of Contents

List of Tables

List of Figures

List of Images

List of Abbreviations

CSD	Critical size defect
FDA	U.S. Food and Drug Administration
RIA	Reamer Irrigator Aspirator ICD
DESTATIS	Federal Statistical Office of Germany
HE	Hematoxylin Eosin
Rt-qPCR	Quantitative reverse transcription polymerase chain reaction
NTC	No reverse transcription control
α-SMA	Alpha-Smooth Muscle Actin
TNF-α	Tumor necrosis factor-α
M-CSF	Macrophage-colony stimulating factor
OPG	Osteoprotegerin
FGF	Fibroblast growth factor
BMP	Bone morphogenic protein
PECAM-1	Platelet endothelial cell adhesion molecule-1
TGFβ-1	Transforming Growth Factor Beta 1

TGFβ-3	Transforming Growth Factor Beta 3
VEGFA	Vascular Endothelial Growth Factor A
IM	Intramedullary
FRET	Fluorescence resonance energy transfer
LW	Tap water
HCL	Hydrochloric acid
RT	Room temperature
EtOH	Ethanol

Abstract

Critical size defects have various causes, including blunt or penetrating trauma, tumor resection, or infection. In addition, the complication of developing a non-union is an constant risk in the healing process.

A retrospective study from 2018-2021 on the number of surgeries for the treatment of non-unions in the Department of Orthopedics and Trauma Surgery at Charité Campus Virchow shows that 10% of all surgeries in Berlin and 0.5% of surgeries in Germany are performed here. During the same period, 6 individuals were operated on in the Department of Orthopedics and Trauma Surgery of Charité Campus Virchow using a specific technique based on the induced membrane technique with satisfactory results, as shown by the case series.

There are several surgical approaches to achieve bony union, and one of them is the induced membrane technique also known as the Masquelet membrane, presented by Alain-Charles Masquelet. In this technique, a spacer is implanted into a bone gap, causing a membrane to develop around it. The spacer is then removed, while preserving the membrane, and replaced with an autologous cancellous bone graft. This membrane acts as a barrier that protects the graft from the environment and graft resorption, causes secretion of osteoinduction growth factors, is a osteogenesis promoting mesenchymal stem cell source, and allows revascularization of the graft from the intraluminal side of the membrane. This membrane is thought to perform similar functions to those of the periosteum, which encases the bone.

After fracture, the periosteum is activated and is highly involved in the complex bone healing process. In this work, histological and expression analyses were performed to compare inactivated, unchanged periosteum, activated periosteum after fracture, and the induced membrane.

The results confirmed similarities between activated periosteum and the induced membrane in terms of their cellular activity and expression, suggesting functional similarities between these two tissue types and that the induced membrane behaves somewhat like activated periosteum, although the membrane morphologically presents as a mirror-inverted arrangement compared with the periosteum. For PECAM-1, TGFβ-1, and TGFβ-3, the expressions are similar. This is confirmation that ongoing research

aimed at providing a membrane comparable to the periosteum, which is available at the first surgery to treat bone defects, has potential for providing a future treatment option.

Abstract Deutsch

Defekte kritischer Größe haben verschiedene Ursachen, darunter stumpfe oder penetrierende Traumata, Tumorresektionen oder Infektionen. Darüber hinaus ist die Komplikation der Entwicklung einer Non-union ein ständiges Risiko im Heilungsprozess. Eine retrospektive Studie von 2018-2021 über die Anzahl der Operationen zur Behandlung von Non-union in der Klinik für Orthopädie und Unfallchirurgie der Charité Campus Virchow zeigt, dass 10% aller Operationen in Berlin und 0,5% der Operationen in Deutschland hier durchgeführt werden. Im gleichen Zeitraum wurden in der Klinik für Orthopädie und Unfallchirurgie der Charité Campus Virchow 6 Personen mit einer speziellen Technik auf der Basis der induzierten Membran operiert, mit zufriedenstellenden Ergebnissen, wie die Fallserie zeigt.

Es gibt mehrere chirurgische Ansätze, um eine knöcherne Vereinigung zu erreichen, und einer davon ist die Technik der induzierten Membran, auch bekannt als Masquelet-Membran, die von Alain-Charles Masquelet vorgestellt wurde. Bei dieser Technik wird ein Platzhalter in einen Knochenspalt implantiert, so dass sich eine Membran um ihn herum entwickelt. Der Platzhalter wird dann unter Beibehaltung der Membran entfernt und durch ein autologes Spongiosa Knochentransplantat ersetzt. Diese Membran fungiert als Barriere, die das Transplantat vor der Umgebung und der Resorption des Transplantats schützt, die Sekretion osteoinduzierender Wachstumsfaktoren bewirkt, eine die Osteogenese fördernde Quelle mesenchymaler Stammzellen darstellt und die Revaskularisierung des Transplantats von der intraluminalen Seite der Membran aus ermöglicht. Es wird angenommen, dass diese Membran ähnliche Funktionen wie das Periost, das den Knochen umhüllt, erfüllt.

Nach einer Fraktur wird das Periost aktiviert und ist in hohem Maße an dem komplexen Knochenheilungsprozess beteiligt. In dieser Arbeit wurden histologische Untersuchungen und Expressionsanalysen durchgeführt, um inaktiviertes, unverändertes Periost, aktiviertes Periost nach Fraktur und die induzierte Membran zu vergleichen.

Die Ergebnisse bestätigten Ähnlichkeiten zwischen aktiviertem Periost und der induzierten Membranen in Bezug auf ihre zelluläre Aktivität und Expression, was auf funktionelle Ähnlichkeiten zwischen diesen beiden Gewebetypen hindeutet und darauf,

dass sich die induzierte Membran in gewisser Weise wie ein aktiviertes Periost verhält, obwohl sich die induzierte Membran morphologisch als spiegelverkehrt im Vergleich zum Periost darstellt. Bei PECAM-1, TGFβ-1 und TGFβ-3 sind die Expressionen ähnlich. Dies ist eine Bestätigung dafür, dass die laufende Forschung, die darauf abzielt, eine dem Periost vergleichbare Membran bereitzustellen, die bei der ersten Operation zur Behandlung von Knochendefekten zur Verfügung steht, das Potenzial einer zukünftigen Behandlungsoption hat.

1. Introduction

According to the Federal Statistical Office of Germany, the number of accidents with severe injuries has stagnated at a similarly high level in the last ten years (1). The increased risk of a bony injury in a motorcycle accident is well known, due to the substantial physical forces that act on the victim's extremities during the impact, which may eventually lead to a critical size defect. Due to the sparse soft tissue coverage of the lower limb, with the resulting limited blood supply to the bone, tibia fractures are especially in danger of developing a non-union. However, besides blunt or penetrating trauma, tumor resections and infections are the leading causes of bone loss. To salvage such limbs, complex surgical reconstructions must be performed to regrow bone and achieve bony stability. This work aims to provide a compact review of the current understanding of bone defects and the resulting non-unions. At the same time, it deals with the biology of fracture healing and introduces surgical options focusing on Masquelet's method. Furthermore, I compare intact periosteum, damaged periosteum and Masquelet membrane via gene expression analysis and immunohistochemical analysis.

1.1 Definition of a critical size defect

To date, no uniform definition of critical size bone defects (CSD) has been established. CSDs have been shown to occasionally heal spontaneously in long bones (2). However, it must be taken into account that a compromised state of the surrounding soft tissue and vascularization may significantly affect the regenerative ability of the bone. For a definition of a critical size defect, the authors Court-Brown et al. suggest a bone loss of >50% of the cortical diameter and a fracture gap of >1cm in length (3). Contrary to this, Sanders et al. postulated that the definition of a critical size defect with a fracture gap of at least 1cm, involving at least 50% of the cortical diameter was not in fact critical (4). Animal model studies usually refer to a different definition of a CSD than in clinical studies. Recently, Sato et al. revised their definition of a CSD to be the smallest bone defect, which does not heal spontaneously during the study span (5). However, this implies that simple fractures might not recover if the study period chosen is short enough. Thus, this definition is not suited for repeatability. A more pragmatic definition was given by Schmitz

et al. They define a CSD in animal studies as one that would not heal during the animal's lifetime (6).

Consensus exists that a critical size defect:

- Does not heal without intervention
- Is larger than 1cm and a loss of > 50% of the circumference
- May require repeated interventions or complex reconstruction to achieve healing

The etiology encompasses various injury mechanisms such as high energy trauma, gunshot or blast wounds, infections, and tumors (2). However, the treatment options are mainly based on the location and the extent of the defect rather than the underlying pathology (7). Schemitsch et al. compared the findings of Hinsche et al. (8) and Keating et al. (9), analyzing the different outcomes of femoral and tibial CSDs. While satisfactory results were observed in the femur, tibial CSDs were less satisfactory, although the mean defect size was smaller. The authors suspected the differences in soft tissue coverage of the femur compared to the tibia (with the less bony blood supply) to be responsible (10). Hence, multiple factors influence the treatment decision, such as the etiology, location of defect, soft tissue state and other factors. A healing method that is universally applicable for a CSD, considering the many factors involved, is the Masquelet Membrane. The magic of this induced membrane will be described in the course of the paper.

1.2 Physiology of bone healing

The physiological processes during bone healing after trauma are finely balanced and leave tiny margins for deviation without compromising the entire process (11).
Following the trauma, fracture healing starts with the hematoma phase, which sets a template for the callus formation (12). Since blood vessels are torn apart and the blood flow is disrupted there is a cessation of oxygen supply and the injured site becomes hypoxic (13). This results in the first phase of fracture repair in form of an acute inflammatory response, in which chemotactic effects recruit other inflammatory and mesenchymal cells promoting angiogenesis and enhancing extracellular matrix synthesis

(14). One of these agents is vascular endothelial growth factor (VEGF), which promotes angio- and vasculogenesis to ensure revascularization and again establishes blood supply (13). During the early hematoma phase, pro-inflammatory stimuli initiate the biological response to the damage, followed by a shift from a pro-inflammatory environment to an anti-inflammatory environment, which is essential for local regenerative processes to develop further. Schmidt-Bleek et al. showed that a prolonged inflammatory response in the early hematoma phase subsequently delays the angiogenic processes and interferes with successful bone healing (14).

The neovascularization following a fracture is required for O_2 homeostasis, delivery of nutrients, removal of catabolic products, and distribution of cells and mediators to the damaged region. This process of neovascularization can be distinguished between angiogenesis (blood vessels forming from pre-existing ones) and vasculogenesis (capillary formation from endothelial progenitor cells) (14). Angiogenesis occurs more frequently as a neovascularization process because new blood vessels tend to sprout and split from pre-existing blood vessels (15). The angioblasts which are involved in vasculogenesis form blood islands which then in turn spread out via angiogenesis. Both these processes thus have a decisive part in a successful neovascularization.

In case of a critical size defect, the soft tissue coverage is often impaired and compromised due to the etiology of the injury, resulting in the injured site being left without existing blood supply or blood vessels to split and sprout from. Thereafter, vasculogenesis plays a crucial role in critical size defects and the process of healing.

Following the hematoma phase, the soft callus phase begins with intramembranous and endochondral ossification (16). During intramembranous ossification, bone evolves from the mesenchymal stem cell subpopulation the skeletal stem cells, which become osteoblasts via the regulation of Runx2 and release Collagen type I. It, in turn, mineralizes and becomes woven bone.

In endochondral bone ossification, the fibrous tissue formed by fibroblasts is replaced by a cartilaginous extracellular matrix, which is synthesized by chondrocytes. These chondrocytes proliferate and calcify the matrix consisting mainly of collagen type II, resulting in soft callus formation (15). Additionally, the aspect of angiogenesis, as mentioned before plays an emphasized role in the process of endochondral ossification, as it mediates the differentiation of avascular cartilaginous tissue into vascularized bony tissue (17).

Moreover, macrophages not only phagocyte inflammatory cells and debris but also participate in the soft callus formation by producing matrix metalloproteases and bone morphogenic proteins (13). Further proliferation and hypertrophy of the chondrocytes results in calcification of the extracellular matrix (12). The resorption of mineralized cartilage is then initiated by an interplay of tumor necrosis factor-α (TNF-α), macrophage-colony stimulating factor (M-CSF), RANKL, and osteoprotegerin (OPG). While the latter three additionally animate the formation of woven bone by osteoblast and osteoclast activation, TNF-α commences chondrocyte apoptosis. This results in mineralization of the callus and replacement by woven bone. Finally, the hard callus and its replacement the calcified cartilage and can be measured with extracellular matrix markers such as type 1 collagen, alkaline phosphatase, osteocalcin and osteonectin. It presents as solid and mechanically rigid bone.
The transformation of the woven bone into lamellar bone accomplishes the final step to achieve the biomechanical properties of a normal bone with a central medullary cavity.

An unstable fracture fixation may lead additionally to a decreased stimulation of osteoblastic differentiation and ultimately inadequate ossification as well as to an imbalance of angiogenic and anti-angiogenic factors, and subsequently to lower expression of the angiogenic factors VEGF and fibroblast growth factor 2 (FGF2), resulting in impaired healing in an atrophic non-union compared to a stable fixation (16).

1.3 Complications resulting in non-unions

Non-unions have been previously defined similarly to CSDs, i.e., no healing without further intervention, independent from the treatment time (18). However, this definition suggests a subjective rather than an objective evaluation which has its limits in a standardized approach. The U.S. Food and Drug Administration (FDA) defined a non-union as a fracture that is not healed within the first nine months after injury and shows no healing progress for at least three months (19). This might help the treating physician, because it defines an overall time frame and one for healing progress. The different stages of a delayed union, non-union and the final stage of pseudoarthrosis are not strictly separated, but rather a merging process (20). Our group summarized several risk factors

for the development of non-unions, such as advanced age, alcohol abuse, malnutrition, smoking, and comorbidities like type 2 Diabetes Mellitus or Cushing's disease. Furthermore, fracture-related factors, the surgical treatment, and biomechanical properties of the implants play a significant role in the occurrence of a non-union (21). Giannoudis et al. introduced the diamond concept, which in addition to proper vascularity includes four key players critically involved in fracture healing: osteogenic cells, osteoconductive scaffolds, growth factors, and the mechanical environment. A lack of these may shift a sufficient fracture healing into an impaired one (22).

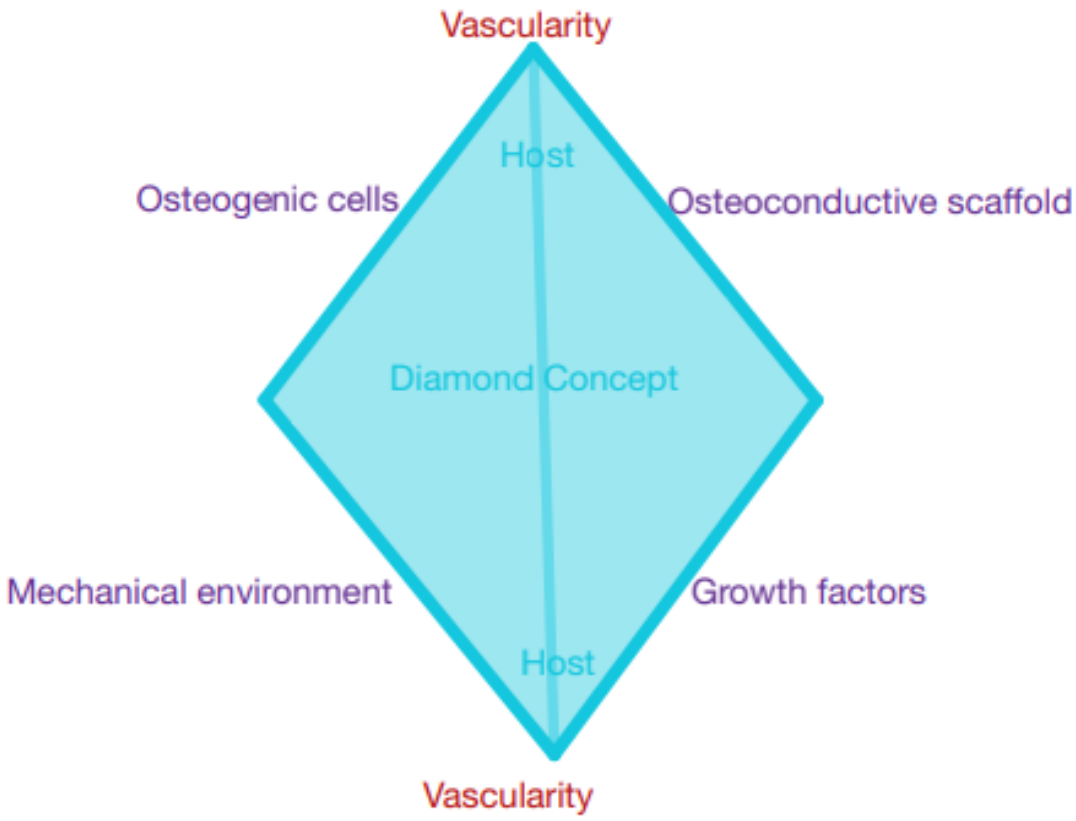

Figure 1 illustrates the "diamond concept" by Giannoudis et al. (22).

Based on the work of Weber and Cech, one can distinguish between three types of non-unions (23):

- Hypervascularity/hypertrophic non-unions
- Avascular/atrophic non-unions
- Infected non-unions

A rich blood supply characterizes hypervascular non-unions, which are thus suited to undergo biological reactions and heal eventually. This type of non-union develops if there is a pronounced amount of micromotion at the fracture site due to mechanical instability (poor biomechanical conditions). To prevent this development, one must optimize the fixation to increase the axial and shear stiffness to a scale conducive to bone formation (24). Hypervascular non-unions can be treated by increasing the stability of the osteosynthesis (21).

Avascular non-unions typically result from reduced or even non-existing blood supply. This might be based on avital bone parts remaining in the fracture site following surgery (20). Such an environment is at high risk of getting colonized by bacteria. Hence, cases of atrophic non-unions can either be based on an avascular or infected situation. Once diagnosed, they require a radical debridement of avital tissue, followed by a stable osteosynthesis and an autologous bone graft for void filling (21).

Most often, infected non-unions appear as complex cases (significant defects, malreduction, multiple prior surgeries, insufficient soft tissue coverage). Patients complain about severe pain, loss of function, and sometimes the development of fistulas. These cases often need an interdisciplinary treatment approach, which involves eradicating the infection by antimicrobial therapy and surgical debridement, bridging the non-union area, reconstructing soft tissues, and stabilizing the fracture (21). Surgical debridement of a non-union – especially infected cases – may result in a CSD.

As emphasized by Gomez-Barrena et al., there is a clear, distinct difference in the genesis of non-union vs CSD. Non-unions show an impairment at the cellular and molecular signaling levels and/or biomechanical weakness, and usually present without a bone gap. In contrast, CSDs present sufficient biological factors, but bone tissue cannot be regenerated across the significant gap due to various reasons, including patient-related factors (25).

1.4 The role of the periosteum in successful healing, non-unions and defects

“All that lives must be protected by an envelope” (26), a poetic description of natural phenomena by Johann Wolfgang von Goethe and, in terms of bone, very true. The

periosteum as well as the induced membrane both have the function of an envelope supporting and protecting the underlying tissue.

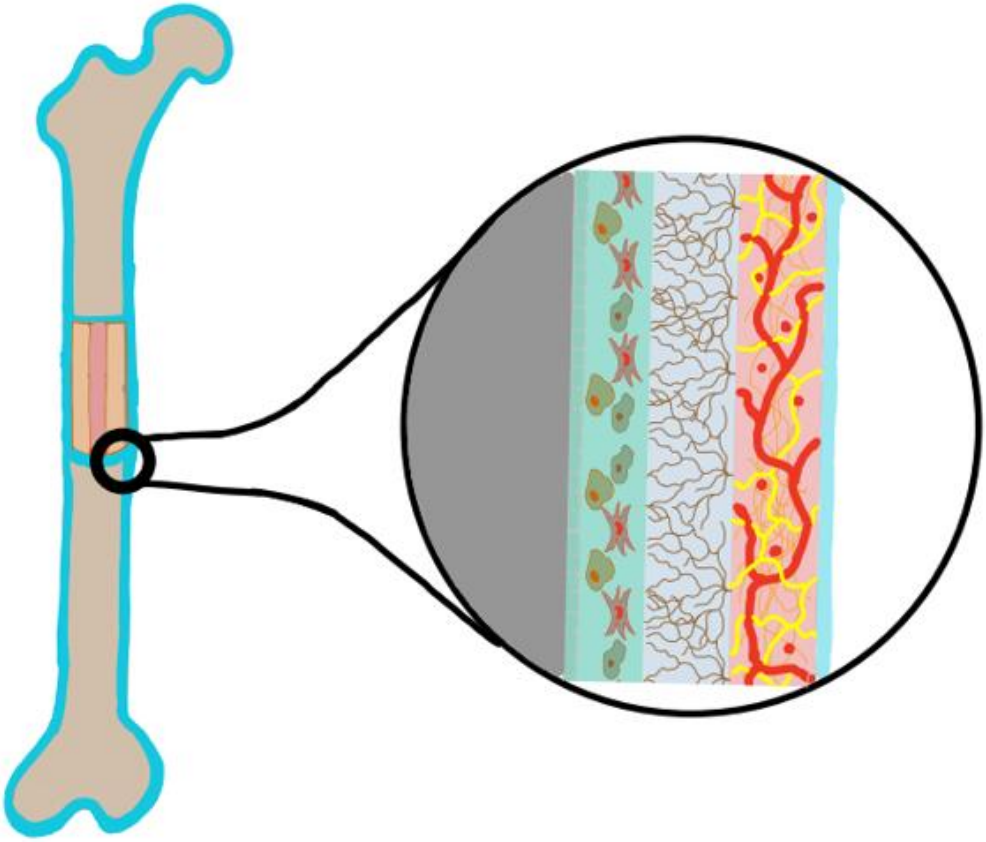

Figure 2 illustrates the periosteal layers (27). The outermost superficial layer on the right shows extracellular matrix consisting of collagen, blood vessels and nerves. In the middle is the fibrous layer with elastic fibers and Sharpey's fibers and the innermost layer is the cambium layer, with mesenchymal stem cells, differentiated osteogenic progenitor cells, osteoblasts, fibroblasts, and endothelial cells.

The periosteum encompasses most of the bones, aiding significantly in fracture healing. The outer periosteal layer consists of two parts (28). The superficial layer consists mainly of an extracellular matrix comprised of collagen and a few elastic fibers. It is highly vascularized, providing the most significant blood supply to the bone. The total blood supply of the periosteum consists of four vascular systems, being the intrinsic periosteal systems, periosteocortical anastomoses, and musculoperiosteal and nutritive periosteal system granting 1/3 of the bone's blood supply (29). Furthermore, it has a rich neuronal

network, with some nerves penetrating the bone cortex and other nerves terminating in the deeper outer layer of the periosteum, the so-called fibroelastic layer. This layer is less vascularized than the superficial layer but is significantly elastic. The Sharpey's fibers, which extend towards the outer cortex to establish a connection with tendons and ligaments, are located here (30). Two types of Sharpey's fibers exist: the horizontal fibers are situated in inserting muscle bundles to realize the biomechanical exchange across the periosteum. The perpendicular fibers add complexity to the muscle-to-bone interface, and influence bone atrophy, augmentation, and remodeling.

The other layer is the inner cambium layer, which is named based on a comparison to a layer of tree bark. Mesenchymal progenitor cells, differentiated osteogenic progenitor cells, osteoblasts, and fibroblasts are concentrated here (21), representing the primary origin of the progenitor cells required for fracture repair (31), as well as endothelial pericytes, which have osteoblastic potential and act as an ancillary source of progenitor cells. While this cambium layer is the thickest in the fetus, it becomes thinner with age and eventually cannot be distinguished from the outer fibrous layer (28). The cambium layer enables appositional bone growth in adolescents and may even allow complete bone regeneration after injury, as seen in "banana peel injuries" of the clavicle in adolescents (32). This injury is defined by a traumatic dislocation of the bone out of the periosteal sleeve, where it remains, while a secondary clavicle might form within the periosteal sleeve. In the case of missing periosteum, the bone healing is significantly delayed, but not entirely prevented, showing the importance of intact periosteum in fracture sites for recovery (28).

The periosteal-derived fracture healing only occurs in sites covered by the periosteum (28), and furthermore, there are differences in osteogenic and chondrogenic capacity of the periosteum depending from which sites of the body it originates, and in that intramembranous and endochondral ossification varies greatly with this periosteal tissue source (33). Hence, different sites in the human body differ in the dominant ossification process. The long bones in the arm and leg express a dominated endochondral ossification, whereas mandibular or cranial bones undergo intramembranous ossification (33). Although the high osseous regenerative capacity of the periosteum somewhat diminishes with age, the reaction of the periosteum following injury still provides the foundation of the fracture healing process (34).

The formation of a hematoma after a fracture will cause the periosteum to institute a chain of events to establish connections to the bone ends. (35). The periosteal layer initiates membranous ossification at the vascularized fragment ends, allowing new bone formation with a good blood supply even in the periphery (28). At the center of the fracture site, where the blood supply is insufficient, the cambium layer is responsible for cartilage production, undergoing endochondral ossification and neo-angiogenesis. This periosteal reaction concludes by the generation of subperiosteal new bone, the establishment of soft callus, and finally, the formation hard callus (28).

The fracture will cause the release of platelet-derived growth factors and fibroblast growth factors which cause the periosteal osteoprogenitor cells to proliferate. Then, within the inflammatory response during fracture repair, interleukin-1-β and tumor necrosis factor-α are released from macrophages and induce the differentiation of pluripotent cells from the periosteum into osteoclasts for resorption of necrotic bone at the fracture site (35, 36). Periosteum-derived cells also activate bone morphogenic protein 2 (BMP-2), which plays an essential role in bone and cartilage growth by being involved in the osteogenic mechanisms like the Wnt/β-catenin signaling for regulation of cellular functions like proliferation, differentiation or stem cell renewal, fibroblast growth factor 2 for mediating the formation of new blood vessels, and the hedgehog signaling process, which amplifies the healing process (37). The activated hedgehog signaling aids periosteal callus formation by influencing osteogenic and chondrogenic differentiation of periosteum-derived cells in alliance with BMP-2 (29). The bone morphogenic protein is regulated by the Wnt signaling pathway and its role becomes clear in case of deletion of BMP2 during fracture repair, as the callus formation is annulled. The bone morphogenic proteins are multifunctional growth factors which are part of the transforming growth factor beta superfamily and not only play a role in embryonic development and cardiac development but also heavily in bone formation (38). The BMP-2 causing the periosteal-derived cells to differentiate into osteogenic cells is positively influenced by the transcriptional regulators Runx2 and Osx. In contrast, there is COX-2 expression, which negatively influences the BMP-2 expression but is also essential in the periosteum derived cell differentiation (29). TGF-β is also abundantly expressed in the periosteum, influencing proliferation and differentiation of periosteum-derived cells as well as participating in Wnt signaling for osteoblast differentiation and even activating the β-catenin signaling pathway (39).

During the inflammation process at the fracture site, cyclooxygenase II and BMP are produced, which affect periosteal mesenchymal cells, increasing their susceptibility for differentiation into osteoblasts according to Neagu et al. Additionally, pluripotent mesenchymal cells in the cambium layer of the periosteum are stimulated by insulin-like growth factors, transforming growth factor-β-1 and fibroblast growth factor 2, to participate in chondrogenesis (35). These complex interactions of periosteum derived pluripotent stem cells provide the cellular foundation for bone healing (36).

Besides the biochemical and signaling pathways during fracture healing, mechanical stimuli significantly influence the healing process as well. The osteoprogenitor cells in the periosteum respond to micromotions in the form of tension and shear forces (35). Those motions are converted into signaling molecules to modulate collagen fibril production, and influenced by further compressing or stretching forces to undergo chondrogenesis or osteogenesis. The mechanical stimulus influences the formation and remodeling of bone, a postulation made already in 1892 by Julius Wolff, which is today known as Wolff's law. It states that bone that bears weight remodels at a higher rate (40). This shows the importance of mechanical micromotions in supporting bone healing, as highlighted in the evolved diamond concept related to Wolff`s law. The initial diamond concept postulated by Giannoudis et al. included four key players critically involved in fracture healing: osteogenic cells, osteoconductive scaffolds, growth factors and the mechanical environment (22). In addition of these and in form of an evolved diamond concept, Willie et al. stress the importance of mechanical stimuli for the regeneration cascade, including influences such as fixation stability, interfragmentary strain, fracture gap size, muscle and soft tissue support, and osteoconductive scaffold or extracellular matrix (16). The latter two are presented as the superordinate elements that serve the other properties of the fracture repair mechanism, such as growth factor release, angiogenesis, cell differentiation, and migration, as well as inflammation under itself by transferring the mechanical stimuli as signals to the cells. Only the correct balance of fracture repair response will result in endogenous tissue regeneration, whereas a misbalance may decrease regeneration potential and might end up in complications such as a non-union.

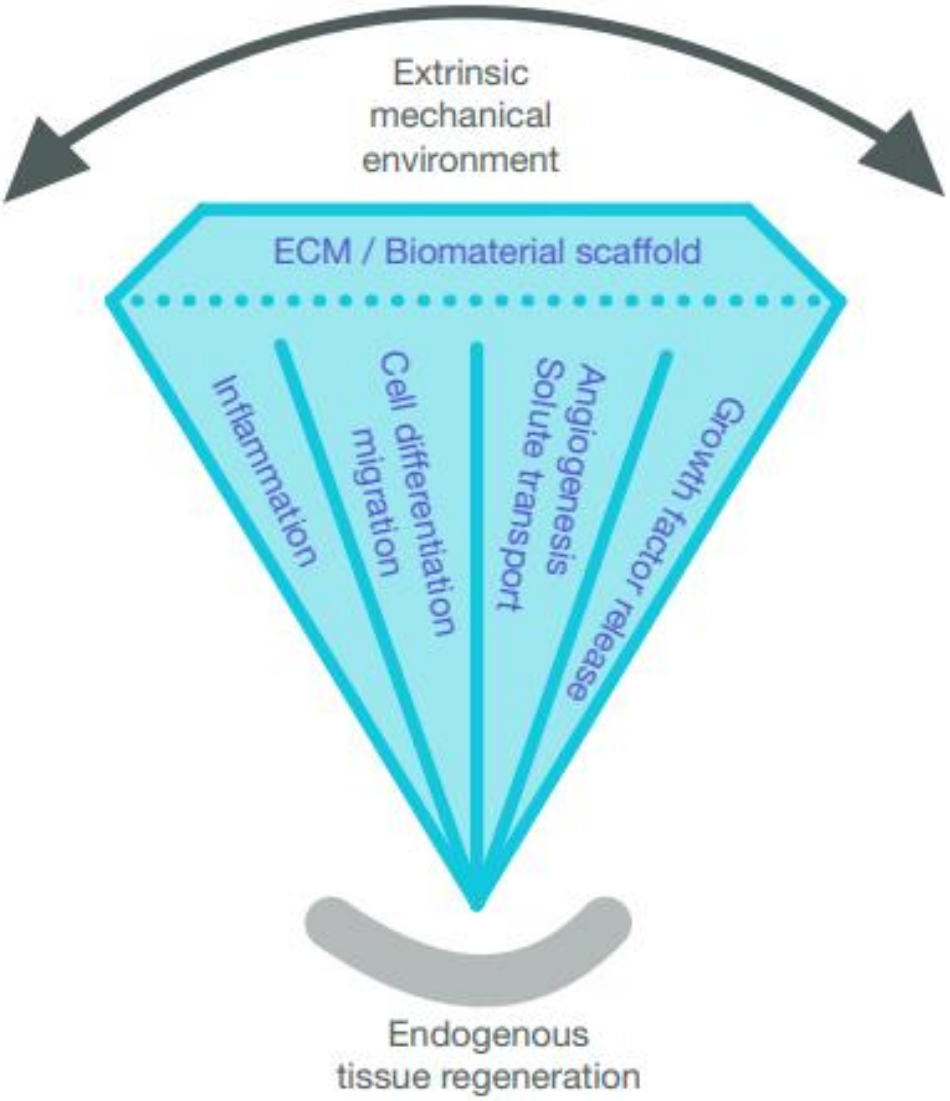

Figure 3 illustrates the evolved diamond concept according to Willie et al. (16).

1.5 Treatment options for critical size defect

The final goal of any reconstruction is to enable osteoinduction, osteoconduction and osteogenesis for the total repair of a bone defect. Albrekston et al. reported different aspects of osteoinduction and osteoconduction, which are the essentials of the bone healing process. Osteoinduction describes the stimulation of undifferentiated pluripotent cells to develop into bone-forming cell lineage, while osteoconduction is the capability and possibility of bone to grow on a surface (41).

Several patient-related factors influence the treatment of a CSD. These include the physiological condition, shape, and location of the defect, surrounding soft tissue, bone quality, deformity, and joint involvement. However, other factors such as the surgeon's experience or the surgical infrastructure also influence the treatment of a defect of critical size (42). In addition, there is currently no effective pharmacological treatment that allows fractures to heal and injured bone to consolidate (43). However, in a clinical setting, it is always important to anticipate and prevent the potential complications, e.g. the development of a non-union when regenerated bone fails to grow together with the original ends of the defect (44).
From a clinical perspective, different techniques have been established to accomplish the successful healing of a CSD.

1.5.1 Segmental bone transport

Prof. Gavriil Abramovich Ilizarov introduced segmental bone transport for the treatment of infected fractures and bone defects over 60 years ago (45). After necessary debridement, which is a prerequisite for all surgeries, in this procedure an osteotomy is performed in the healthy bone away from the defect, resulting in a free bone segment comprising one end of the defect (46). This free bone segment is subsequently transported through the defect, slowly reducing its size while new bone forms at the expanding osteotomy site. An external ring fixator performs stabilization of both the bone and the segment transport. This fixator includes adjustable elements, which enable the segment transport, typically at a transportation rate of 1mm per day (47).
The traction forces applied by the fixator act on the bone ends at the osteotomy site, inducing bone regeneration on the surface of the distracted bone, featuring a central radiolucent fibrous interzone comprised of type 1 collagen (47). From this central collagen zone, new bone trabeculae develop, eventually causing callus formation and consolidation (48).
The Ilizarov method is reliable in treating CSD with predominantly satisfactory outcomes (49, 50). However, several downsides exist: the requirement for high compliance, discomfort wearing the ring fixator, pin tract infections, and the long duration of the treatment (average treatment duration: 10-11 months) (51). In recent years, telescopic

intramedullary nailing systems have become available, eliminating the need for an external fixator (52). However, the transportation capacity is limited by the length of the expanding telescopic system. Therefore, extended defects may require several surgeries to “re-load” the transportation nail. At the end of the bone transport, a so-called docking site surgery is often needed independently from the transportation method. This docking site surgery is typically combined with removing the transport system and debridement as well as osteosynthetic stabilization of the docking site with additional bone graft application. Several surgical variations of transport procedure have been published so far. Mathieu et al. stress the importance of additional intramedullary nailing in extended tibia defects to prevent secondary loss of alignment (53). Some authors advocate using additional intramedullary stabilization in femoral defects due to the higher forces that have to be withstood during bone transport (53). However, it has to be kept in mind that intramedullary nailing options are only feasible in some instances, as in the process the existing vasculature is further destroyed, risking, for example, not only the development of non-unions but also infections. This omnipresent risk of infection remains a major complication in surgery. Regarding fracture-related infection, Bezstarosti et al. compared in a meta-analysis the most common treatment modalities for a critical size defect. These were autologous cancellous bone with and without local antibiotics, the induced membrane technique, vascularized grafts, and segmental bone transport with and without local antibiotics (54). They found that a recurrence of infection did not significantly differ between the different treatment options with overall comparable healing rates. This furthermore highlights the importance of sufficient debridement and the risk of infections irrespective of the chosen treatment method. New methods are constantly being developed and improved, such as the intramedullary nail lengthening, which can not only be used as an addition, but also alone be used and there are currently different implanted intramedullary nails available. Mechanical nails were the first to be used and further improved by the forms of motorized and magnetic nails. Despite different methods, all three show satisfactory treatment results. The continuous improvement of the bone lengthening technique using the intramedullary nail reduces the use of an external fixator and the patient has an increased quality of life and satisfaction on top of a reduced complication rate (55).

An additional approach which reduces the adverse effects of externally placed fixation devices is plate-assisted bone segment transport with motorized lengthening nails and

locking plates, a technique presented by Olesen et al. in 2019 (56). After successful debridement and soft tissue refurbishment, a corticotomy is carried out generating the vascularized bone segment for transportation. The medullary canal of the bone is reamed, and the abraded tissue invades surrounding soft tissue at the distraction site. Then, the intramedullary lengthening nail is inserted, while the plate with blocking screws reinforces stability. After docking of the segment, a secondary surgery is recommended for debridement of the bone ends, together with autologous cancellous bone graft insertion. According to Olesen et al. the application is currently limited to femur and tibia, but has a comparable healing rate to other bone healing methods and allows earlier weight bearing due to the high solidity of the assembly, because this method relies on many screws in the locking plate in addition to the intramedullary nail, which also constitutes a major downside of this method as there is no room for adjustments or correction once the transportation is initiated (57). Since the method is newly implemented into the conglomerate of fracture healing methods, it may after all prove to be a very useful tool for the treatment of bone defects. However, further research and observation is required.

1.5.2 Bone graft

Bone grafting can be accomplished via many different approaches, depending on the cause, location, size of defect and more. The application of bone grafting may be either used in combination with another method for bone reconstruction or solely as the primary reconstructive intervention itself.

The main differentiation is between vascularized and non-vascularized bone graft.

Vascularized bone grafts are available in two forms, firstly free vascularized bone grafts, where the donated bone is cut off from its original blood supply, and upon transplantation, anastomosed to local blood supply (58). The other form is the pedicled vascularized bone graft, where the blood supply is not interrupted but rather the donor bone is brought to the recipient location. In this case, it is necessary that the donor site is in proximity of the graft site.

The most common bone grafts used are non-vascularized autologous bone grafts, where patients' bone is harvested from a donor site (10). The iliac crest represents the gold standard harvesting site, because it allows access to cancellous, cortical, or combined

grafts. Although it is an excellent graft, with low donor site morbidity except pain and discomfort in the extraction site, it is limited by the amount of bone available. Alternatively, a cancellous bone graft can be obtained from long bones like the femur or tibia by a Reamer Irrigator Aspirator (R.I.A., DePuy Synthes) to harvest autologous bone (18).

The advantages of autologous bone grafting are that the graft contains the patient's characteristics, osteogenic cells and osteoinductive proteins (e.g., BMP2, PDGF), which provide osteoinductive and osteoconductive properties without foreign body cells or added growth factors (59).

Vascularized bone grafts (e.g., fibula), represent a versatile reconstructive method applicable to various indications. They may be used solely or in conjunction with an allogenic bone graft to reconstruct long bones and are well established for the reconstruction of the jaw, both with standard and customized implants (60). In young adolescents, the proximal fibula in conjunction with its articulate surface at the proximal tibiofibular joint may even be used for biological reconstruction of a femoral head (61).

Allografts represent a further option. These grafts are available as fresh frozen grafts or decellularized freeze-dried grafts (62). Allografts overcome autograft limits by providing sufficient graft material even for significant segmental defects (63). They are immediately available in all shapes and sizes if a local bone bank is available (64). However, the disadvantages of allograft when compared to autograft are that the foreign body cells have limiting effects on osteoinductive and osteoconductive properties (65)**.**

Xenografts represent a third option for bone grafts. Contrary to autografts/allografts, they are harvested from different species, such as bovine or porcine xenografts (59). Xenografts are highly available and have an optimal porosity for bone tissue ingrowth and sufficient strength. However, like allografts, the significant disadvantage is the absence of osteoinductive properties, which are needed for optimal healing (66).

An approach to combine the advantages and overcome disadvantages of the two potent options of autograft/allograft would be using a combination of autologous and allogeneic graft. It could sufficiently be used in large segmental defects, while not depleting the patient's available tissue, and filling whole defects with favorable cells providing osteoinduction and osteoconduction (59).

1.5.3 Induced membrane

As described by Alain-Charles Masquelet, the induced membrane technique, also called the Masquelet technique, in its essence, is still performed in the same way even 30 years after its inception (67). After successful control of a possible underlying infection, two surgical procedures are required.

The first step begins with a thorough debridement. The defect is then filled with bone cement and, to ensure the membrane covers the entire defect site, it is important that the cement overlaps the defects by 1cm (68), then bony stability is obtained with a bridging plate construct. Before the second surgical intervention, a membrane forms around the cement filler. This newly formed membrane contains angiogenesis- and osteogenesis-related growth factors, like vascular endothelial growth factor α, bone morphogenic protein 2, and transforming growth factor β -1. Because this membrane involves different immune effector cells associated with angiogenesis, it is considered as a unique bioreactor (69).

It can be assumed that the induced membrane mimics the function of the periosteum, thus promoting biological fracture healing.

Optimal conditions for the membrane to support bone growth are reached after four weeks as the highest vascular and osteoinductive levels are measured (68). However, the membrane might be too fragile to be incised and thus could be damaged in the process of the removal of the cement spacer. Hence, six to eight weeks following this first step procedure, the membrane formed is durable enough to be incised without destroying it (70). However, different authors have shown that the results of treatment are satisfactory even outside of this time frame (71, 72). In a second surgery, the membrane is incised, the spacer is removed, and the defect is filled with autologous bone graft, typically harvested from the iliac crest or as described above via R.I.A. (73).

As Masquelet summarized, there are four key elements of the membrane (74).

1. A functioning barrier (protection from the environment and from graft resorption)
2. Secretion of osteoinduction growth factors
3. Osteogenesis promoting mesenchymal stem cell source
4. Graft revascularization from the intraluminal side of the membrane

A significant advantage of this technique is that it doesn't require any advanced materials to heal a critical bone defect (53) or an extraordinarily high amount of extra materials. Furthermore, it is highlighted by Choufani et al. in their study about using the Masquelet technique in austere environments in Africa, that given the severity of damage, it is an readily performable surgical intervention even in settings with limited medical equipment or resources (75). Irrespective of the etiology of a CSD, the induced membrane technique can be used as a universal treatment option. While bone healing is achieved almost independently of the defect size, a six to eight centimeter defect length might be the limit of highly successful healing upon treatment with the induced membrane (53), but there are reports of successful treatment of up to 25cm of defect length (67).

The possible downsides and limitations of this technique are summarized by Mathieu et al. into septic, mechanical, and biological (53):

1. Septic: complete eradication and proper debridement in case of necrotic, contaminated, or infected tissue is essential in the induced membrane treatment; additionally, sufficient soft tissue coverage and antibiotic treatment is required. Infection represents the highest rate of complications. Therefore, it can be necessary to debride repeatedly to control the infection before definitive surgery (76). It might be preferable to use external fixation until the eradication of the infection. The temporarily used external fixation prevents the occurrence of a bacterial biofilm on internal fixation devices (77).
2. Mechanical: insufficient stability causes non-union and implant failure and must be avoided by providing sufficient stability of bone fixation as well as sufficient intramedullary cavity filling. The reduction of risk of mechanical failure is highly dependent on the intraoperative awareness of the surgeon.
3. Biological: failure of graft revascularization due to excessive bone substitutes; additional application of growth factors with the possible competition reaction with the ones produced by the induced membrane (53).

When taking all the factors into account when approaching the treatment of a CSD, the induced membrane technique represents a very suitable technique for reconstruction (74). However, it is only applied in approximately 11.5 % of all CSD cases according to Bezstarosti et al. (54). In a study done by Karger et al. in 2012, they retrospectively analyzed 84 long bone defects treated with the induced membrane technique, in which the defect size was above 5cm in 48 cases and had a total defect size range of 2- 23 cm. The results given showed a bone union in 90% of the cases and amputation in 10% of

the cases due to poor soft tissue coverage after the trauma (78), emphasizing even more that sufficient soft tissue coverage is required for successful healing of the defect.

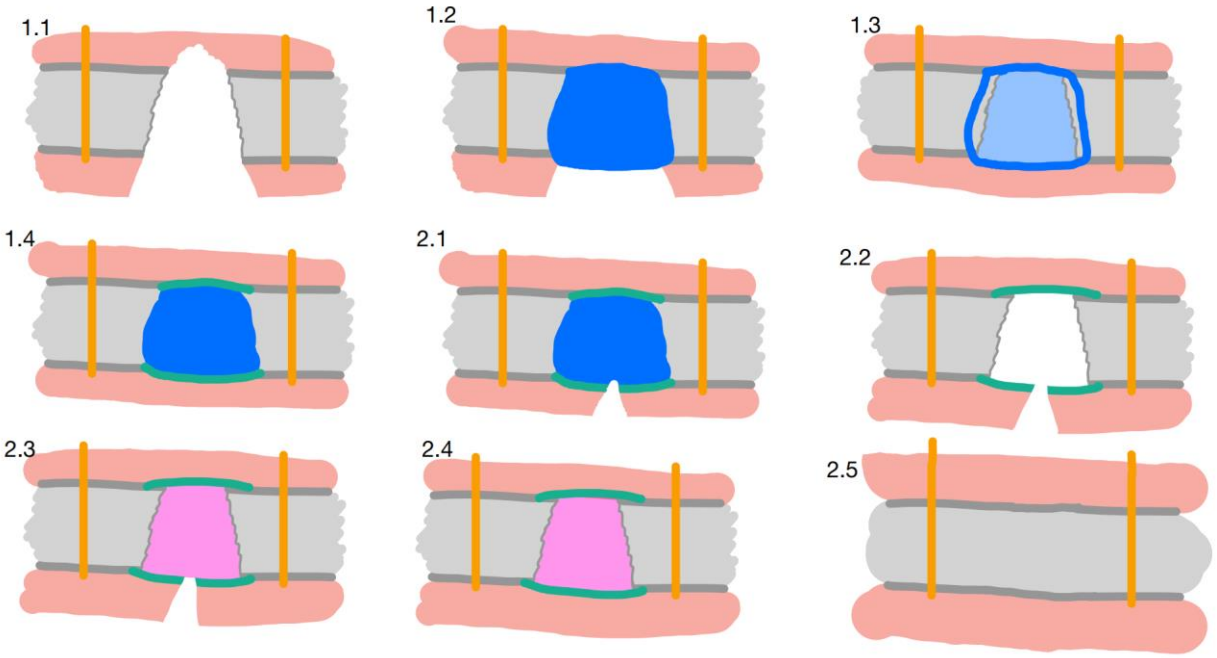

Figure 4 illustrates the principle of the induced membrane technique. 1.1 Shows the injury and the loss of bone and soft tissue. After debridement, the PMMA spacer is inserted in 1.2. 1.3 Shows the overlapping of the bone by the cement spacer with sutured skin. 1.4 Shows the forming membrane in green after the first step. 2.1 Represents the second step of the operation. Small incision of membrane is followed by removal of the cement spacer in 2.2. In 2.3, bone marrow is implanted and the skin is sewn up in 2.4. In 2.5, the bone is finally consolidated.

1.6 Retrospective analysis of M84.1

The goal of the analysis was to find out how many critical size defects / pseudarthroses are being operated on in the Department of Orthopedics and Trauma Surgery of the Charité Campus Virchow clinic and to especially find out how many times the induced membrane technique was applied together with its success rate. Furthermore, these

results were compared with the data provided by the Federal Statistical Office of Germany (“Destatis”).

There are two different International Classification of Diseases (ICD10) coding systems for identification of diseases, one being the 3-coded system, which indicates the broad pathology, while the other more detailed 4-coded system indicates detailed information on the pathology. For the retrospective analysis, the number of cases in Germany and Berlin with the 3-coded ICD10 M84 diagnosis being disorders of continuity of bone and with the 4-coded ICD10 M84.1 diagnosis being non-union of fracture (Pseudoarthrosis) were reviewed. As mentioned, the 3-coded ICD-10 code of M84 stands for disorder of continuity of bone without any further subclassification. Hence, many pathologies, will find inclusion in the statistics and increase the numbers of cases. A more detailed statistical result is found for the 4-coded ICD 10 code M84.1, which stands for pseudoarthrosis. Naturally, the number of cases is smaller in the more detailed 4-coded ICD10 statistic.

Unfortunately, there were no data for the M98.7 code, which stands for major osseous defects (79). It would be very interesting to see the number of cases for this pathology as one possible operating technique for this pathology is the induced membrane technique, but since it is not used in German but only in American ICD-10 coding no data are available here.

An overview of ICD-10 codes M84 and M84.1 shows their codes and respective meanings. These pathologies found inclusion into the statistics of the Federal Statistical Office of Germany “Destatis”. Already, from these two different tables, one can appreciate the reason for the different numbers of recorded cases.

Table 1 Three-coded ICD-10 M84: Disorders of continuity of bone (80)

M84. 0 Malunion of fracture
M84. 1 Non-union of fracture (Pseudoarthrosis)
M84. 2 Delayed union of fracture
M84. 3 Stress fracture, not elsewhere classified
M84. 4 Pathological fractures, not elsewhere classified
M84. 8 Other disorders of continuity of bone
M84. 9 Disorders of continuity of bone, unspecified

Table 2 Four-coded ICD-10 M84.1: Non-union of fracture (Pseudoarthrosis) (81)

M84.10 Non-union of fracture	multiple sites
M84.11 Non-union of fracture	shoulder region (clavicle, scapula, acromioclavicular, glenohumeral, sternoclavicular joint)
M84.12 Non-union of fracture	Upper arm (humerus, elbow joint)
M84.13 Non-union of fracture	forearm (radius, ulna, wrist)
M84.14 Non-union of fracture	hand (finger, carpus, metacarpal, joints between these bones)
M84.15 Non-union of fracture	pelvic region and thigh (pelvis, femur, buttocks, hip, hip joint, sacroiliac joint)
M84.16 Non-union of fracture	lower leg (fibula, tibia, knee joint)
M84.17 Non-union of fracture	ankle and foot (tarsus, metatarsus, toes, ankle joint, other joints of the foot)
M84.18 Non-union of fracture	Other (neck, head, ribs, trunk, skull, spine)
M84.19 Non-union of fracture	site unspecified (unspecified localization)

Results of the Federal Statistical Office of Germany “Destatis”

The two ICD-10 code pathologies that are presented here are M84 – Disorders of continuity of bone, and M84.1 – Non-union of fracture (Pseudoarthrosis) for the years 2019, 2018 and 2017 in Germany and Berlin, because the data were the most recent - statistics and results for 2020 were not released at the time the work was conducted. The study includes the period of the last 3 years to be able to relate the evaluated surgical results to the current state of affairs and not to earlier pathological and surgical techniques and definitions that have gone out of fashion. Since the pathology of M89.7 - Major osseus defect is not used in Germany, no results for either 4-coded or 3-coded ICD-10 are included. According to “Destatis”, the following numbers of ICD-10 diagnosis in the years 2019 (82), 2018 (83) and 2017 (84) were released.

Table 3 Four-coded ICD-10 Main Diagnosis, age (<18) and sex in Germany in the years 2019, 2018 and 2017

Year	ICD-10	Male	Female
2019	M84.1	7,324	5,578
2018	M84.1	7,204	5,432
2017	M84.1	7,555	5,434

Table 4 Three-coded ICD-10 Main diagnosis, sex in Germany and Berlin in the years 2019, 2018 and 2017

Year	ICD-10	Germany		Berlin	
		Male	Female	Male	Female
2019	M84	12,257	11,427	584	603
2018	M84	11,932	10,913	576	465
2017	M84	12,405	11,071	580	472

One can appreciate the respective distribution of the M84 diagnosis within Germany in the years 2019, 2018 and 2017. The results throughout the three years appear to be very similar in total diagnosis in Germany as well as in regional diagnosis in Berlin.

In all three years, the age was presented in the case of 4-coded ICD but not 3-coded ICD10. Hence, in the case of the 4-coded ICD 10 main diagnosis, patients under the age of 18 years were excluded from the statistic since they were indicated. However, in the 3-coded ICD 10, patients below the age of 18 could not be identified because they were not indicated. They were excluded because in the analysis of operations within the orthopedics and trauma surgery of the Charité Campus Virchow clinic only patients of legal age were included.

Furthermore, one can see that in three years Berlin had 3,280 operations under the M84 code with a similar female/male ratio and a slightly higher number for men.

The same applies for Germany over the analyzed three years, where a similar ratio with a tendency towards higher case numbers for men can be seen.

For the retrospective analysis about the surgeries performed at the Charité Campus Virchow, all surgeries were considered that were performed at the Charité Campus Virchow clinic from 10.01.2018-01.01.2021 in the orthopedics and trauma surgery of the Charité Campus Virchow clinic with the abbreviation “WUC-OP”. In total, the operations

amounted to 14,517. Among these, a search for the number of operations were performed under the same ICD-10 code as “Destatis” with the following results:
Regarding M84 Disorders of continuity of bone there were 325 operations.
More specifically for the ICD 10 code M84.1 – Non-union of fracture (Pseudoarthrosis), there were 209 cases during the years that were analyzed. For the long bones, there were 114 cases, from which the pelvic region and thigh were 37, the lower leg 39, the humerus 20 and the forearm 20 cases. In the statistical enumeration, the pelvic region and the femur are used as one ICD-10 code, namely as M84.1 5. Since there are no long bones in the pelvic region, only the femur, and not the pelvic region, was included for the code M84.1 5 in the cases examined in the department of orthopedics and trauma surgery at the Charité Campus Virchow clinic.

Table 5 Cases from 10.01.2018-01.01.2021 in orthopedics and trauma surgery of the Charité Campus Virchow clinic

M84.11 Non-union of fracture	Shoulder region	20
M84.12 Non-union of fracture	upper arm	20
M84.13 Non-union of fracture	forearm	20
M84.14 Non-union of fracture	hand	22
M84.15 Non-union of fracture	pelvic region and thigh	37
M84.16 Non-union of fracture	lower leg	39
M84.17 Non-union of fracture	ankle and foot	43
M84.18 Non-union of fracture	other	1
M84.19 Non-union of fracture	site unspecified	1

In order to accurately compare the data with the aforementioned data from “Destatis”, it would be preferable to compare the exact same years, as there was no data about 2020 from “Destatis” at the time the study was conducted.
Unfortunately, no statement can be made about a comparison with the more precise number of performed M84.1 surgeries, as there are no data provided by “Destatis” about Berlin specifically.
However, regarding M84.1 surgeries compared with all cases in Germany within the last three years, the orthopedics and trauma surgery of the Charité Campus Virchow clinic covered 0.5% of them.

1.7 Induced membrane case series

In the last three years, the Masquelet technique was relied on in six patients in the orthopedics and trauma surgery of the Charité Campus Virchow clinic. This case series highlights the success that Charité had when this technique was applied.

1. A 31-year-old male patient sustained a complex lower leg fracture of the distal tibia in a traffic accident, coded as S82.3, and was treated with an intramedullary (IM) nail in another hospital. For a year, as a complication, an infected non-union of the tibia with an anterior cortical defect developed, coded as M84.16. This was treated by hardware removal and debridement of the tibia, removal of the intramedullary nail, and extensive irrigation. Following bone debridement, a defect size of 7cm remained. This void was filled with bone cement, representing stage 1 of the Masquelet technique. Nine weeks later, stage 2 was performed by harvesting autologous cancellous bone from the left femur and supported with an intramedullary nail. The patient was discharged from the hospital in good general condition. Unfortunately, there are no follow-up records, as the patient did not originate from Germany and returned to his home country. The time from the initial diagnosis until the 2nd step of the Masquelet membrane technique was 15 months.

2. A 53-year-old male patient sustained a subtrochanteric femur fracture during a motorcycle accident, which was treated with a dynamic hip screw in another hospital. However, non-union and implant failure occurred.
The dynamic hip screw was removed, followed by a brief debridement of the bone. This led to a 3.5 cm defect which was bridged with bone cement. The bone was stabilized after open reduction of the multifragmentary fracture using a reamed IM nail.
Nine weeks later, the 2nd step of the Masquelet technique took place with bone grafting from the pelvis and femur shaft. The six-month follow-up revealed minor complaints of the muscle of the right thigh. Eight weeks after the 2nd step, full weight bearing was allowed. At that time, X-ray showed that the bone transplant was not yet completely consolidated but a callus was present. After twelve months, moderate complaints were still reported, and X-ray controls documented complete consolidation. The time from the initial diagnosis until the 2nd step of the Masquelet membrane technique was five months.

3. A 62-year-old male patient suffered a polytrauma with III° distal open femur fracture and decollement of the upper and lower leg. Initially, the patient was treated by closed reduction and external fixation of the femur. One week later, open reduction and internal fixation with a locking plate were performed. In the course of this a non-union developed. After thorough debridement the 6 cm long bone defect was bridged with bone cement. Eight weeks later the 2nd step of the Masquelet technique was performed, with bone grafting from the right femur and additionally, stabilization with a plate osteosynthesis. Follow up after twelve months showed consolidation in the X-ray. The time from the initial diagnosis until the 2nd step of the Masquelet membrane technique was 6 months.

4. A 45-year-old male patient sustained a shrapnel injury to the proximal tibia and was treated with multiple surgical interventions using the Ilizarov procedure in a non-EU country during the first year after injury. Two years later, plate osteosynthesis was applied in another German Hospital. Another two years later, due to recurrent soft tissue infections, wound healing disorders and shortening of the leg, non-union of the tibia was diagnosed. This was treated with debridement, plate osteosynthesis and implantation of bone cement into the 1cm tibial defect as the 1st step of the Masquelet membrane technique. Eight weeks later, the 2nd step of the Masquelet technique was applied. The 1-year follow-up shows stable conditions and no further dynamics despite partial implant failure. The patient used forearm crutches only for subjective reasons. In the follow-up after 14 months, only a filiform delineable gap in the tibia was visible in the X-ray. Subjectively, there was a clear improvement, and the use of crutches was discontinued. The time from the initial diagnosis until the 2nd step of the Masquelet membrane technique was six years.

5. A 63-year-old female patient sustained a distal tibia fracture treated by plate osteosynthesis. After nine months, the developed chronic multifocal osteomyelitis of the tibia was diagnosed. This was treated with debridement and the 1st step of the Masquelet membrane technique. Eight weeks later, the 2nd step of the Masquelet membrane technique with autologous cancellous bone harvest from the femur and, additionally, plate osteosynthesis was performed. The bone gap size was not documented. The six-months follow-up showed increasing consolidation. Two years after the second step of the

Masquelet membrane technique, X-ray control revealed consolidation of the bone defect, as well as indication for plate removal. The time from the initial diagnosis until the 2nd step of the Masquelet membrane technique was 11 months.

6. A 68-year-old male patient sustained a III° open tibia fracture which was primarily treated with double plate osteosynthesis. An infectious non-union developed in the tibia. This was treated by removal of the tibial plates, and extensive irrigation. After debridement, a 1.7cm bone gap remained, which was filled with bone cement according to the 1st step of the Masquelet membrane technique, as well as re-osteosynthesis of the tibia. Six weeks later, the 2nd step with autologous cancellous bone transplant from the femur was performed. Four-months follow-up showed a subjective well-being at transition to full load bearing. X-ray showed further consolidation and correct implant position. CT scan showed medial plate thickening and yet incomplete consolidation. In the follow-up after 14 months, X-ray showed a line drawing in the callus area without signs of non-union. 18 months after, the clinical stability with a pain-free gait was assumed, as the patient reported to be subjectively pain and discomfort free. The time from the initial diagnosis until the 2nd step of the Masquelet membrane technique was 2.5 years.

In case of complications like non-unions, or severe defects or situations in which recovery seemed allegedly beyond retrieval, it proved to be a reliable treatment alternative, if all else failed. This case series of patients treated with the induced membrane technique shows that it is a successful and satisfactory treatment method. Despite not being the first treatment of choice, like plate osteosynthesis or transport nails are, the induced membrane technique can be relied on. When it is used, a high success rate of treatment of the defects has been achieved. Although plate osteosynthesis or intramedullary nail transport are widely used, there are clinical situations in which the options to resort to these surgical procedures are limited. For example, complications of the aforementioned surgical treatments, infections, persisting non-unions, or extremely large bone defects. In medicine generally, it is important to be able to offer treatment alternatives, especially if the classical and primarily preferred strategies have not led to success. Clinically, it is important to be able to motivate the patient and point out a goal and, as the treating

physician, to be able to fall back on a reliable method for difficult cases. This is provided by the induced membrane technique.

2. Methodology

The explorative, descriptive study was conducted in the Julius-Wolff-Institute, Berlin from 14.1.2021-1.5.2022. A total of five patients were included in the studies. Written informed consent was obtained from all study participants and research was carried out in compliance with the Helsinki Declaration. Research approval and ethics clearance were acquired in advance in the form of application number EA2/199/1, Human Research Ethics Committee.

Two patients admitted to orthopedics and trauma surgery of the Charité Campus Virchow for treatment of the lower extremity after fibular fracture were invited to participate in this study. During fracture repair of the fibular bone, the activated periosteum was obtained. The material is discarded routinely but was collected for the research purpose of this study. The tissue harvest thereby presented no additional damage, risk, or burden for the patient.

Two patients admitted to the Mund-Kiefer-Gesichts-Chirurgie-Department of the Benjamin-Franklin–Faculty of Charité Berlin who underwent bone transplant surgery from the fibular to mandible were included in my study. During this surgery, a bony segment from the fibular is routinely discarded, but in the case of this research it was collected, likewise without additional burden, damage, or risk for the patient.

One patient had the cement spacer removed, but a different choice of therapy followed than the 2nd step of the induced membrane. Therefore, the membrane was removed and instead of being discarded, it was collected for my study and thereby presented no additional damage, risk, or burden for the patient.

2.1 Gene expression

Gene expression analyses were performed to analyze the cellular response to the changing environment after a bone fracture.

For transparent and comprehensive results of our quantitative reverse transcription polymerase chain reaction (RT-qPCR), I followed the good practices guidelines thoroughly described in the Nature publication by Bustin et al. in 2013 (85).

2.1.1 RNA Isolation of human tissue

The RNA isolation was achieved by using the RNeasy Mini Kit by QIAGEN according to manufacturer's protocol to ensure RNA quality.
The tissue samples of approximately 0.5cm^2 were obtained with a surgical forceps in the operating theater and placed in a 2.0 ml tube, which was immediately transferred into liquid nitrogen (LN2) after receiving the sample to be frozen and then stored in a freezer at -80°C. For RNA isolation, I used the RNeasy Mini Kit provided by QIAGEN. The sample was taken out of the freezer and crushed in a grinding jar until no intact pieces and only powder was visible, while always assuring the sample was frozen by pouring LN2 in the jar so that it did not defrost. After filling a new 2.0ml tube with the sample powder, LN2 was poured into it as well to keep the sample always frozen. Then, 1ml TRIzol®Reagent and subsequently 200ml chloroform for molecular biology was added and the tube was vortexed. 10 minutes of incubation and 10 minutes of centrifugation at 10,000x g followed. The tube displayed an with the aqueous phase on top, which was placed into a new 2.0 ml tube and the remaining interphase and lower organic phase were discarded. Then, Isopropanol was added in a ratio of 1:2, mixed well and incubated at room temperature (RT) for 10 min. Afterwards, it was centrifuged at 14,000x g for 10 minutes. Then, 500 µl 75% EtOH was added to the sample in the tube and mixed well. Next, the column was loaded with a maximum of 700 µl of the sample, followed by centrifugation for 30 sec at 10,000x g at 4°C. The flow was discarded, but I continued to use the tube and repeated this step if there was still sample left. I loaded the column with the remaining sample and centrifuged for 30 sec at 10,000x g at 4°C, and again discarded the flow-through. Then, I added 350 µl buffer RW1 to the column (wash step), followed by centrifugation for 30 sec at 10,000x g at 4°C, and I discarded the flow-through. Next, I added 80 µl DNase mixture carefully to the column, if possible in the center directly on the membrane, and incubated it for 15 minutes at RT. Then, I added another 350 µl buffer RW1 to the column (wash step), centrifuged it for 30 sec at 10,000 x g at 4°C, and discarded the flow-through. Next, I added 500 µl buffer RPE to the column (wash step) and centrifuged it for 30 sec at 10,000x g at 4°C, and discarded the flow through. Then, I added another 500 µl buffer RPE to the column (wash step), and centrifuged it for 2 minutes at 10,000x g at 4°C, and discarded the tube. Then, the column was placed in a new 2 ml tube without a lid and centrifuged for 1 minute at maximum speed at 4°C to achieve drying of the membrane,

and the tube was discarded. Finally, the column was transferred into a new 1.5 ml tube. I carefully added 30 µl H2O, which was heated by the heating block to 60°C onto the column, preferably centered on the membrane, incubated for 5 minutes at RT and centrifuged for 2 minutes at 10,000x g at RT. Lastly, I put the column into a new 1.5 ml tube and closed the other tube well, as it was the final result of the RNA isolation. To obtain another tube, I again added 30 µl H2O from the heating block, carefully onto the column, if possible, in the center on the membrane, which was placed in a new tube, incubated for 5 minutes at RT, and centrifuged for 2 minutes at 10,000x g at RT. The column then was discarded, and the tube closed well. Finally, I vortexed the samples well. For storage, of the samples were stored in freezer at -80°C.

Table 6 Materials/ Reagents/ Equipment and Sources for RNA Isolation

Material/ Reagent / Equipment	Source
Liquid Nitrogen	
TRIzol®Reagent	Invitrogen
Chloroform for molecular biology	VWR
Ethanol for molecular biology	VWR
RNeasy Mini Kit	QIAGEN
RNase Free DNase Set	QIAGEN
Nuclease Free Water	QIAGEN
Descosept	Charité
RNase AWAY®	VWR
Fume hood	
Patient Pad, 40 x 60	Charité
Cotton gloves	A. Hartenstein
Dewar transport vessel, 3l	VWR
Crucible tongs	VWR
Ladle	Roth
Crush Set (Cup und Punch)	Charité/ Werkstatt
Rubber mallet	

Microspoon	Roth
Pipette, variable, 0.5 - 10 µl	eppendorf (research)
Pipette, variable, 10 - 100 µl	eppendorf (research)
Pipette, variable, 100 - 1000 µl	eppendorf (research)
Dualfilter-Tips, 0.5 - 20 µl	eppendorf
Dualfilter-Tips, 2 - 100 µl	eppendorf
Dualfilter-Tips, 50 - 1000 µl	eppendorf
DNA LoBind Tubes 1.5 ml	VWR
DNA LoBind Tubes 2.0 ml	VWR
Vortex Shaker VV3	VWR
Heraeus™ Microcentrifuge Fresco™ 17	VWR
Block thermostat SBH130D with blocks for 1.5 und 2.0 ml tubes	VWR

2.1.2 Photometric measurement

To prepare the next step, I measured the RNA concentration, which I isolated from our tissue sample using photometric measurement (by Implen P-class P360). 1 µl of the isolated RNA from the previous step was used for this analysis.
The ratio of absorbance values of 260nm/280nm as well as the purity was supposed to show if there was a contamination with proteins, since its presence would alter the ratio. The purity should range from 1.8-2.1 to be pure. The Results are visible in Table 12.

Table 7 Materials/ Reagents/ Equipment and Sources for photometric measurement

Nuclease Free Water	QIAGEN
BioPhotometer	eppendorf
UVette	eppendorf
Pipette, variable, 0.5 - 10µl	eppendorf (research)

Pipette, variable, 10 - 100µl	eppendorf (research)
Dualfilter-Tips, 0,5 - 20µl	eppendorf
Dualfilter-Tips, 2 - 100µl	eppendorf

Table 8 Results of photometric measurement

	1. Run		
	ng/ µl	260/ 280	260/ 230
1.1	1980	2.004	1.692
2.1	1512	2.060	2.370
3.1	1430	2.109	2.134
4.1	1516	2.123	2.032
5.1	534	2.046	2.068
6.1	122	2.054	1.912
7.1	1218	2.057	1.952
8.1	34.8	2.023	1.450
9.1	30.4	2.000	0.894
10.1	14.4	1.714	0.070
11.1	5.2	1.300	0.295
12.1	22.4	1.931	0.789
13.1	7.2	1.636	0.818

Maximum absorption was set with a wavelength of 260nm.

2.1.3 Reverse transcription of RNA into cDNA

After RNA isolation, I applied the iScript™ cDNA Synthesis Kit by Bio-Rad as the first step in the two-step reverse transcription quantitative PCR (RT-qPCR). Therefore, I calculated the amount of RNA serving as a template that I needed to convert into sufficient complementary DNA (cDNA) for our RT-qPCR.

After calculation, 1 µg of total RNA of each sample was then used for cDNA synthesis with the iScript Reverse Transcription SuperMix for RT-qPCR.

For the cDNA generation I followed the steps in the protocol of iScript™ cDNA Synthesis Kit provided by Bio-Rad. The kit included the reagent 5x iScript reaction mix, iScript Reverse transcriptase as well as nuclease free water.
For the mixture, a 0.5ml DNA LoBind tube was firstly filled with 5x iScript Reaction mix, then with nuclease free water, then the RNA and lastly the iScript reaction mix, all with the precalculated volumes. Then, the tube was incubated in the MASTERCYCLER. The thermal cycler underwent priming for 5 minutes at 25°C, reverse transcription for 20 minutes at 46°C, and RT inactivation for 1 minute at 95°C. In order to increase the volume of the cDNA to be enough for the wells of the transparent optical reaction plate in the next step, 40 µl nuclease free water were added to result in the tube being filled with 80µl.
The cDNA samples could now be used in reverse transcription quantitative PCR (RT-qPCR)

Table 9 Materials/ Reagents/ Sources for reverse transcription of RNA into cDNA

Material/Reagent	Source
iScript™ cDNA Synthesis Kit	Bio-Rad
Pipette, variable, 0.5 - 10 µl	eppendorf (research)
Pipette, variable, 10 - 100 µl	eppendorf (research)
Dualfilter-Tips, 0.5 - 20 µl	eppendorf
Dualfilter-Tips, 2 - 100 µl	eppendorf
DNA LoBind Tubes 0.5 ml	VWR
Vortex Schüttler VV3	VWR
PCR-Cooler	eppendorf
Centrifuge MiniSpin®	eppendorf
Mastercycler® gradient	eppendorf

2.1.4 Reverse transcription quantitative polymerase chain reaction

In the reverse transcription quantitative polymerase chain reaction (RT-qPCR), detection of mRNA is monitored in real time during its course. It visualizes the quantitation during the process, rather than the final product at the end. This allows one to see the amplification progress of a target and allows one to detect the first amplifications. The

higher the initial copy number of the nucleic acid target, the earlier a significant increase in fluorescence is observed. This allows to draw a conclusion towards the different concentration rates of the targets within the tissue sample.

For detection, I used the method with hydrolysis probes (TaqMan probe) depending on fluorescence resonance energy transfer (FRET) (86). This causes a signal emission prevention via the quencher of the dye as long as the probe is intact. The hydrolysis probes are designed to bind downstream of the qPCR primers. The 5’ end is labeled with a fluorescence marker, while on the 3' end, there is a quencher molecule preventing fluorescent emission when near the reporter. Because of the DNA polymerase, the primer is extended, and the probe is cleaved, removing the quencher molecule from the fluorescence marker. This allows the reporter molecule to emit a fluorescent signal, which in turn can be analyzed. After preparation of the Hydrolysis probes (TaqMan probe), the next step can be followed.

Table 10 Equipment and Sources used for RT-qPCR

Equipment	Source
Quantstudio™	
Centrifuge with plate adapter	
Microcentrifuge	
Pipette, variable, 0.5 - 10µl	eppendorf (research)
Pipette, variable, 10 - 100µ	eppendorf (research)
Dualfilter-Tips, 0.5 - 20µl	eppendorf
Dualfilter-Tips, 2 - 100µl	eppendorf

Table 11 Hydrolysis Probes (TaqMan)

Reagent	Source
TaqMan Fast Advanced Master Mix-1 x 5 mL	Life Technologies
Oa04655196_m1	Thermo Fisher/ Charite
Oa04825272_gH	Thermo Fisher/ Charite

Oa04744383_m1	Thermo Fisher/ Charite
Oa04677159_m1	Thermo Fisher/ Charite
Oa04259484_m1	Thermo Fisher/ Charite
Oa04911276_m1	Thermo Fisher/ Charite
Oa04804209_m1	Thermo Fisher/ Charite
Oa04653812_m1	Thermo Fisher/ Charite
Bt03224616_g1	Thermo Fisher/ Charite
Bt03230412_g1	Thermo Fisher/ Charite

Table 12 Preparation of PCR reaction mix

	Volume in 1 well
n=	1
TaqMan® Fast Advanced Master Mix	10
TaqMan®Assay	1
Nuclease Free Water	7
Volume without cDNA -> NTC	18
cDNA Sample	2
Volume with cDNA	20

The next two steps for the RT-qPCR begin with the preparation of the wells. I used the MicroAmp® optical 96-well reaction plate from Life Technologies. The correct amount of volume was transferred from the tubes into each well of the transparent optical reaction plate. Then, 2 µL cDNA was added to the first three wells of a six-well row for a certain hydrolysis probe. Afterwards, the plate was sealed with optical adhesive film, then centrifuged for 1 minute at 400rpm turns to bring the PCR reaction mix to the bottom of the well and to eliminate bubbles. The distribution of the well plate is visible in Table 17.

Table 13 Well distribution of the transparent reaction plate

	1	2	3	4	5	6	7	8	9	10	11	12
A	HPRT1	HPRT1	HPRT1	HPRT1	HPRT1	HPRT1	TGFB3	TGFB3	TGFB3	TGFB3	TGFB3	TGFB3
	1_1	1_1	1_1	H_2O	H_2O	H_2O	1_1	1_1	1_1	H_2O	H_2O	H_2O
B	PPIA	PPIA	PPIA	PPIA	PPIA	PPIA	VEGFA	VEGFA	VEGFA	VEGFA	VEGFA	VEGFA
	1_1	1_1	1_1	H_2O	H_2O	H_2O	1_1	1_1	1_1	H_2O	H_2O	H_2O
C	RPL13A	RPL13A	RPL13A	RPL13A	RPL13A	RPL13A						
	1_1	1_1	1_1	H_2O	H_2O	H_2O						
D	BMP2	BMP2	BMP2	BMP2	BMP2	BMP2						
	1_1	1_1	1_1	H_2O	H_2O	H_2O						
E	NT5E	NT5E	NT5E	NT5E	NT5E	NT5E						
	1_1	1_1	1_1	H_2O	H_2O	H_2O						
F	PECAM1	PECAM1	PECAM1	PECAM1	PECAM1	PECAM1						
	1_1	1_1	1_1	H_2O	H_2O	H_2O						
G	TGFB1	TGFB1	TGFB1	TGFB1	TGFB1	TGFB1						
	1_1	1_1	1_1	H_2O	H_2O	H_2O						
H	TGFB2	TGFB2	TGFB2	TGFB2	TGFB2	TGFB2						
	1_1	1_1	1_1	H_2O	H_2O	H_2O						

Since the probes were target specific, I could be sure that they showed our Targets of Interests (TOI). For the TOI's, I applied TaqMan probes to show BMP2, which is a marker for Osteogenesis, the growth factor markers VEGF, TGF 1-2-3, as well as the probe for CD31, which is a marker for hematopoiesis, and CD73, a marker for Mesenchymal stem cells.

As reference genes to look for errors between the samples, I chose Cyclophilin A as an abundantly occurring protein, Ribosomal 18s-UE which is a part of the ribosomal RNA and the protein Hypoxanthine Phosphoribosyl transferase 1 (HPRT1).

The prepared MicroAmp® optical 96-well reaction plate from Life Technologies was then placed in the RT-qPCR Quantstudio machine.

2.1.5 Analysis of PCR results

The RT-qPCR resulted in an amplification curve with initiation, exponential, and plateau phases. The baseline marks the place where the amplification curve starts (86). When the reaction goes into exponential growth, the fluorescence reaches a value well above the baseline and the threshold level is reached. The set threshold is recorded as a Ct or Cq value and was set to 0.2. The reference gene (housekeeping gene) works as an

endogenous control. As constantly expressed reference genes (87), I used the housekeeping genes: Cyclophilin A, HPRT, and Ribosomal 18s-UE.
Due to the lower amount of RNA found in the samples 6-11, three TOIs/housekeeping genes (HPRT1, NT5E and TGFB2) were omitted after analysis of the initial PCR results of the Masquelet membrane. This was due to their low expression in the Masquelet membrane RT-qPCR as well as in one activated periosteal sample
For relative quantitation, I calculated the ratio between the reference genes (median) and the TOI which is $2^{(-\Delta CT)}$. The Ct of the reference gene is removed from the TOI Ct generating delta Ct for all samples. A graphic created via the program PRISM 9 shows the $2^{(-\Delta CT)}$values.

2.1.6 No-reverse transcription control (NTC)

Suffice to say that good laboratory practice is of high importance when it comes to RT-qPCR amplification, as even small amounts of DNA that might have contaminated the samples lead to false positive amplifications. During laboratory practice I followed the suggestions of the “Applied biosystems 11.202 – TaqMan gene expression assays protocol”. I wore gloves and a clean lab coat, changed gloves when a contamination was suspected, had the equipment stored in different areas, did not bring amplified PCR products into the PCR setup, opened and closed tubes carefully and kept reactions and liquids capped as much as possible, used positive displacement pipettes used solely for PCR, and worked in a clean workplace.
In order to control the samples, nuclease free water was used as a control medium during the RT-qPCR process. Not one of the analyzed tissue samples had a positive water reaction, hence showing that there was no contamination, and the genetic analysis was executed cleanly and carefully.

Workflow Summary provided by “TaqMan Gene expression assays protocol” (88)
Prepare the cDNA sample → Prepare the total RNA → Perform reverse transcription → High-Capacity RNA-to-cDNA Kit → Prepare the reaction mix and load the plate → Prepare the PCR reaction mix → Load the plate → Run the real-time PCR reaction → Create the plate document/experiment → Run the plate → Analyze the results

2.2 Histology and immunohistochemistry

2.2.1 Sample preparation

Since autolysis takes place in the removed tissue samples, it is important to interrupt this process immediately. Therefore, the periosteum samples for the histology and immunohistochemistry were obtained and immediately embedded after in paraformaldehyde solution (PFA) 4% for 2 hours. Then, they were washed with PBS three times and left for 24h in PBS solution. Eventually, the samples were put into 10%-sugar solution, 20%-sugar solution and 30%-sugar solution each for 24, hours respectively. Then, the samples were embedded via the Kawamoto method.

Table 14 Equipment used for embedding in PFA

Equipment
n-Hexan
Dry ice
Dewar flask
Embedding medium (SCEM)
Cryo mould
Tweezers
Silica gel bag for storage
Wooden spatula

N-hexane was filled into the Dewar flask and dry ice was added in sufficient quantity to cool down the hexane and until no more bubbles or vapor formed in the flask. This formed a lake for immersion of the cryoforms. The cryoforms were filled with 4°C cooled SCEM and the tissue sample was placed in the center. By holding the container just above the surface of the n-hexane and eventually complete immersion, the specimen was surrounded by n-hexane/dry ice until it was completely frozen within the SCEM medium. Finally, the cryomould was removed and the cryoblock was stored in a -80°C freezer.

2.2.2 Cryostat

For the work at the cryostat, the following settings were applied:
Bbject holder temperature -23°C to -25°C
Chamber temperature -23°C to -25°C
Cutting thickness 7 um (variable)
Knife angle 2.5° (variable)

Table 15 Materials for cryo section

Material
Blades Feather NHR 35 (variable)
Blades Leica carbide D, separate blade holder required
Blades Leica #TC-65, separate blade holder necessary
Cryofilm type 3C(16UF), Number: C-FUF303 of Section Lab

The previously formed Cryoblocks were taken from the -80°C freezer and placed in cryostat for 30 minutes. Then, the Cryoblock was cut to the desired level which was optimal for staining. Once the level was established, the special Kawamoto foil (cryofilm type 3c(16UF), of section Lab) was placed on the cryoblock via tweezers and pressed on with a spatula to fix it firmly. Then, 7µm thick slices were cut at slow to medium speed. Afterwards, the cut piece was placed on sections on the prepared slides and fixed with adhesive tape still in the cryostat to preserve the cold. Before staining, the sections were freeze-dried for 30 min in the cryostat.

2.2.3 HE-Staining

To stain the cryosections, the sections were first fixed in 4% formaldehyde solution and then rinsed in distilled water. Regressive nuclear staining with the dye hematoxylin was then performed. After the subsequent differentiation step and blueing in tap water, staining in eosin was performed. Eosin is a regressive dye, it is water-soluble and stains cytoplasm, collagen fibers and residual tissue components in different shades of red. This

was followed by a truncated ascending alcohol series (96% EtOH and absolute EtOH), removing the water from the section. The water content in the 96% EtOH acts as a differentiating agent for the eosin. The penultimate step was rinsing in an intermediate (xylene). Finally, the specimen was covered with a medium to produce a microscopic permanent preparation. The section was covered with a covering medium (Vitroclud) and was sealed airtight. After drying in the air, it was protected from mechanical damage and as far as possible, protected from fading.

Table 16 Materials/ Reagents/ Sources for HE staining

Material / Reagent	Source
Formaldehyde 4% buffered pH7 ·1l	SAV Liquid Production GmbH
Xylol, ExtraPure, SLR	Fisher Scientific GmbH
Ethanol	Carl Roth GmbH + Co. KG
Hematoxylin acc. Harris	Merck KGaA
Hydrochloric acid, fuming 37%	Merck KGaA
Eosin, conc. watery 2%	Waldeck GmbH & Co. KG
Vitroclud	R. Langenbrinck GmbH
Acetic acid 100%	Merck KGaA
Tap water	
Distilled water	
Cover glasses strength 1, 24 x 32 mm	Carl Roth GmbH + Co. KG
Cover glasses strength 1, 24 x 40 mm	Carl Roth GmbH + Co. KG
Cover glasses strength 1, 24 x 50 mm	Carl Roth GmbH + Co. KG
Tweezers	
Dye box	Carl Roth GmbH + Co. KG
Dye frame	Carl Roth GmbH + Co. KG
Wire hanger for staining rack	Carl Roth GmbH + Co. KG
Object carrier	Carl Roth GmbH + Co. KG
Measuring cylinder	
Funnel	
Filter paper	
Glass flask	
Vent	

The Preparation of 96% EtOH solution (400 ml), by 16ml distilled water and 384ml absolute EtOH, was well mixed, and stored in an appropriately labeled glass bottle until it was used. The preparation of hematoxylin was a ready-to-use solution, but it was filtered before usage. The preparation of 0.2 % eosin as a ready-to-use solution (200 ml), by dilution of eosin, concentrated water 2% 1:10 with distilled water to a 0.2% diluted solution, 180 ml distilled water and 20 ml of 2% concentrated eosin solution, was well mixed, then 2 drops of glacial acetic acid/ 100 ml diluted solution, i.e., 4 drops, were added and mixed well and stored in appropriately labeled glass bottle until used and filtered before it was used. The preparation of 0.25% HCl ethanol (200 ml), done by dissolving 37% HCl 1:400 in 70% ethanol, 199.5 ml 70% EtOH and 0.5ml of 37% HCl, hydrochloric acid was added to EtOH while stirring, and it was stored in appropriately labeled glass bottle until used.

For sequence, I set up the staining series before staining, labeled the staining boxes and set it up in the following sequence: 1. 4% formaldehyde, 2. distilled water, 3. hematoxylin, 4. tap water, 5. tap water, 6. HCl-EtOH, 7. tap water, 8. tap water, 9. eosin, 10. 96% EtOH, 11. 96% EtOH, 12. absolute EtOH, 13. absolute EtOH, 14. Xylene, 15. Xylene. I placed the vials for xylene and 4% formaldehyde under the fume hood, filled each vial with 200ml of the appropriate solution and closed them with the glass cover.

For the procedure: I sorted the sections to be stained into the staining rack and passed them through the staining series of 14 steps. 1. 4% formaldehyde solution with 2-minute fixation of the section, 2. Distilled water for 2 minutes to rinse off formaldehyde slurry. 3. hematoxylin for 7 minutes for the core dye. 4. Tap water to rinse off the core dye 5. Tap water for 3 minutes to solidify the dye on the nucleus. Microscope control: only nuclei may be stained blue. 6. 0.25% HCl-EtOH with 2x swirl to dissolve the excess dye. 7. Tap water for 10 min to rinse off differentiating agent, with new tap water several times, to solidify the dye on the nucleus and blueing due to slightly basic pH of the tap water. 8. Eosin for 2 minutes for plasma dye. 9. 96% EtOH 2x swirled to rinse and differentiate the dye. 10. 96% EtOH 2x swirled to rinse off and differentiate the dye. 11. absolute EtOH for 2 minutes for dehydration of the sections. 12. abs. EtOH for 2 minutes for dehydration of the sections. 13. Xylene for 2 minutes to dissolve the EtOH. 14. Xylene for 2 minutes to dissolve the EtOH.

General aspects that I took care of were: When I changed the cuvettes, I always dabbed the staining rack on paper towels. After the last xylene step, I covered the sections with Vitroclud, which I did under the fume hood. I removed the section from the staining rack with tweezers and placed it on a towel, dropped some Vitroclud onto the section, then I placed the coverslip carefully on the section with as few air bubbles as possible. I then pressed the cover slip lightly and checked the section again for air bubbles, and again carefully pressed out any remaining air bubbles with the pipette. I placed the sections on a slide tray and allowed them to dry under the fume hood and stored them in a slide box until microscopy.
Concerning staining results: nuclei, cartilage, and calcium appear blue. Plasma in general appears pink. Plasma of muscles appears pink. Erythrocytes appear brick red. Decalcified bone and diseased cartilage appear red.

2.2.4 Immunohistochemistry to identify alpha-smooth muscle actin (α-SMA)

Preparation:
For this procedure it is necessary to prepare some solutions:
70% EtOH solution (200 ml), 80% EtOH solution (200 ml), 96% EtOH solution (400 ml) and phosphate buffer solution (PBS) (2000 ml 1% BSA/ PBS solution), additionally, the blocking buffer in which you mix 5% NS horse/ 1% BSA in PBS solution. Thus, in numbers it would be 9500 µl 1% BSA/ PBS solution + 500 µl NS horse. This must be mixed by carefully pipetting up and down. To prepare the selected primary anti-body α SMA (1:200), one must calculate per section. For one section, 995 µl Antibody Diluent + 5 µl α SMA Antibody is valid. The secondary antibody is horse anti-mouse; This is mixed as follows: 2% AK, 2% NS/ 1% albumin from bovine serum/ PBS solution. This must also be calculated per section. For one section, there is 960 µl 1% BSA/ PBS solution + 20 µl Secondary AK + 20 µl NS. The Antibody - Complex (AK 5000) contains: 1x reagent A (Avidin DH), 1x reagent B (Biotinylated AP). Then, add 2 drops of reagent A and 2 drops of reagent B to 10 ml of PBS solution and mix. This solution must be prepared at least 30 min before use. To prepare the chromogen buffer with pH 8.2, 3.96 g Tris-HCl, 0.54 g Tris-Base, and 2.63 g NaCl are needed. All this is put into a measuring cylinder and dissolved in 150 ml distilled water. The aspired pH value should be 8.2. Then, make up

to 300 ml with distilled water and store at 4°C. To prepare the Substrate Complex (SK 5100), the following contents are required: 1x Reagent 1; 1x Reagent 2; 1x Reagent 3. Add 2 drops of Reagent 1 to 5 ml Chromogenic Buffer and mix. Then, add 2 drops of reagent 2 and mix. Then, add 2 drops of reagent 3 and mix well. This solution should be used quickly. To prepare the 1% methyl green, dissolve 2 g of methyl green in 200 ml of distilled water and add 50 ml of abs EtOH. Finally, mix everything well.

Table 17 Materials/ Reagents/ Sources for staining of α-SMA

Material / Reagent	Source
Xylol, ExtraPure, SLR	Fisher Scientific GmbH
Ethanol	Carl Roth GmbH + Co. KG
Phosphate buffer solution 10x concentrated, pH 7.2	Waldeck GmbH & Co. KG
Normal Horse Serum Blocking Solution	Vector Laboratories, Inc.
Albumin, IgG-free, NZ-Origin	Carl Roth GmbH + Co. KG
Alpha SMA	Agilent Technologies, Inc.
Antibody Diluent, Background Reducing	Agilent Technologies, Inc.
Horse Anti-Mouse IgG Antibody, rat adsorbed (H+L), Biotinylated	Vector Laboratories, Inc.
VECTASTAIN® ABC-AP Kit	Vector Laboratories, Inc.
Vector® Red Substrate Kit	Vector Laboratories, Inc.
Distilled water	
Trizma® Hydrochloride -hydrochloride	Merck KGaA
Trizma®-Base	Merck KGaA
Sodium chloride	Merck KGaA
Methyl green zinc chloride double salt	Merck KGaA
Vitroclud	R. Langenbrinck GmbH
Silicon ring	
Cover glasses strength 1, 24 x 32 mm	Carl Roth GmbH + Co. KG
Cover glasses strength 1, 24 x 40 mm	Carl Roth GmbH + Co. KG
Cover glasses strength 1, 24 x 50 mm	Carl Roth GmbH + Co. KG
Tweezers	
Dye box	Carl Roth GmbH + Co. KG

Dye frame	Carl Roth GmbH + Co. KG
Wire hanger for staining rack	Carl Roth GmbH + Co. KG
Object carrier	Carl Roth GmbH + Co. KG
Measuring cylinder	
Funnel	
Filter paper	
Glass flask	
Vent	

Set up the staining series before staining.

Label staining boxes and set up one after the other:

1. Xylene; 2. Xylene; 3. absolute EtOH; 4. absolute EtOH; 5. 96% EtOH; 6. 80% EtOH; 7. 70% EtOH; 8. Distilled water; 9. PBS; 10. PBS; 11. Methyl green; 12. 96% EtOH; 13 absolute EtOH; 14. absolute EtOH; 15. Xylene; 16. Xylene. It is important to always place cuvettes for xylene under the fume hood and fill 200 ml of the corresponding solution into each cuvette and close with the glass lid.

Preparation of the staining chamber

Line the staining chamber with cloths and then pour distilled water over the cloths. Pour over. Now wait a little until everything is soaked and then pour off the excess water. Perform all incubations in a closed staining chamber.

Procedure

Day 1: 1. PBS for 5 min. to change the medium; 2. PBS for 5 min.

Place sections in the staining chamber, apply a silicone ring around the tissue. These sections must not dry out during this process, keep moist with PBS if necessary. Pipette the solutions directly onto the sections so that they cover the entire section; 3. Blocking for 30 min via non-specific binding; 4. Primary antibody overnight/ 4°C binding of primary Antibody.

Day 2: Remove the sections from wet chamber, remove the silicone rings and place in cuvettes with PBS so that more intense rinsing takes place; 5. PBS for 5 min to rinse off the excess primary antibody; 6. PBS for 5 min. Place the sections in the staining chamber,

apply a silicone ring around the tissue. Make sure that the sections do not dry out - if necessary, keep them moist with PBS. Pipette the solutions directly onto the sections so that they cover the entire section; 7. Secondary AK for 30 min to ensure binding of the secondary antibody to the primary antibody. Remove the sections from the wet chamber, remove silicone rings and place in cuvettes containing PBS. 8. PBS for 5 min to rinse off the excess secondary antibody; 9. PBS for 5 min. Place sections in staining chamber, apply silicone ring around tissue. As always, make sure sections do not dry out in the process, keep moist with PBS if necessary. Pipette the solutions directly onto the sections so that they cover the entire section; 10. AB complex for 50 min to ensure binding of the avidin-biotin-enzyme complex. Remove the sections from the humidity chamber, remove silicone rings and place in cuvettes containing PBS; 11. PBS for 5 min to rinse off the AB complex; 12. PBS for 5 min. Place the sections in the staining chamber, apply a silicone ring around the tissue. Do not allow the sections to dry out, keep moist with PBS if necessary. Pipette the solutions directly onto the sections so that they cover the entire section; 13. Chromogen buffer for 5 min to change the medium; 14. Chromogen buffer for 5 min; 15. Substrate complex for 20 - 30 min; color change occurs. Remove the sections from the wet chamber, remove the silicone rings and place in cuvettes containing PBS; 16. PBS for 5 min to rinse off the substrate complex; 17. PBS for 5 min; 18. Distilled water for 2 min change of medium; 19. Methyl green for 25 min for nuclear staining and counterstaining; 20. 96% EtOH for a short time only to rinse off the color; 21. Abs. EtOH for 2 min to dehydrate the sections; 22. Absolute EtOH for 2 min; 23. Xylene for 2 min to rinse off the EtOH; 24. Xylene for 2 min.

When changing cuvettes, always dab the staining rack on wipes. After the last xylene step, cover the sections with Vitroclud. This is also done under the fume hood. Remove the section from the staining rack with tweezers and place it on a cloth. Now drip some Vitroclud onto the section. Then, carefully place a coverslip on the section, as free of air bubbles as possible, and press the coverslip lightly. Check the section again for air bubbles and carefully press out any remaining air bubbles with the tweezers. Place the sections on a slide tray and allow to dry under the fume hood. Then store in a slide box in the dark until microscopy. The staining result should show the smooth muscle cells in vessel walls as red and the nuclei in green.

As the last step in all procedures, finally, microscopy of the slides was performed using the Leica DM6B microscope.

3. Results

3.1 Histological analysis

Unaltered, undamaged, intact periosteum as well as activated periosteum after fracture and induced membrane were all stained in hematoxylin and eosin staining in order to analyze the tissue structure and cell composition.

3.1.1 Histological analysis of unaltered periosteum

The periosteum is clearly visible between the bone layer as well as the muscular and connective tissue layer. In the inactivated status it appears very thin.

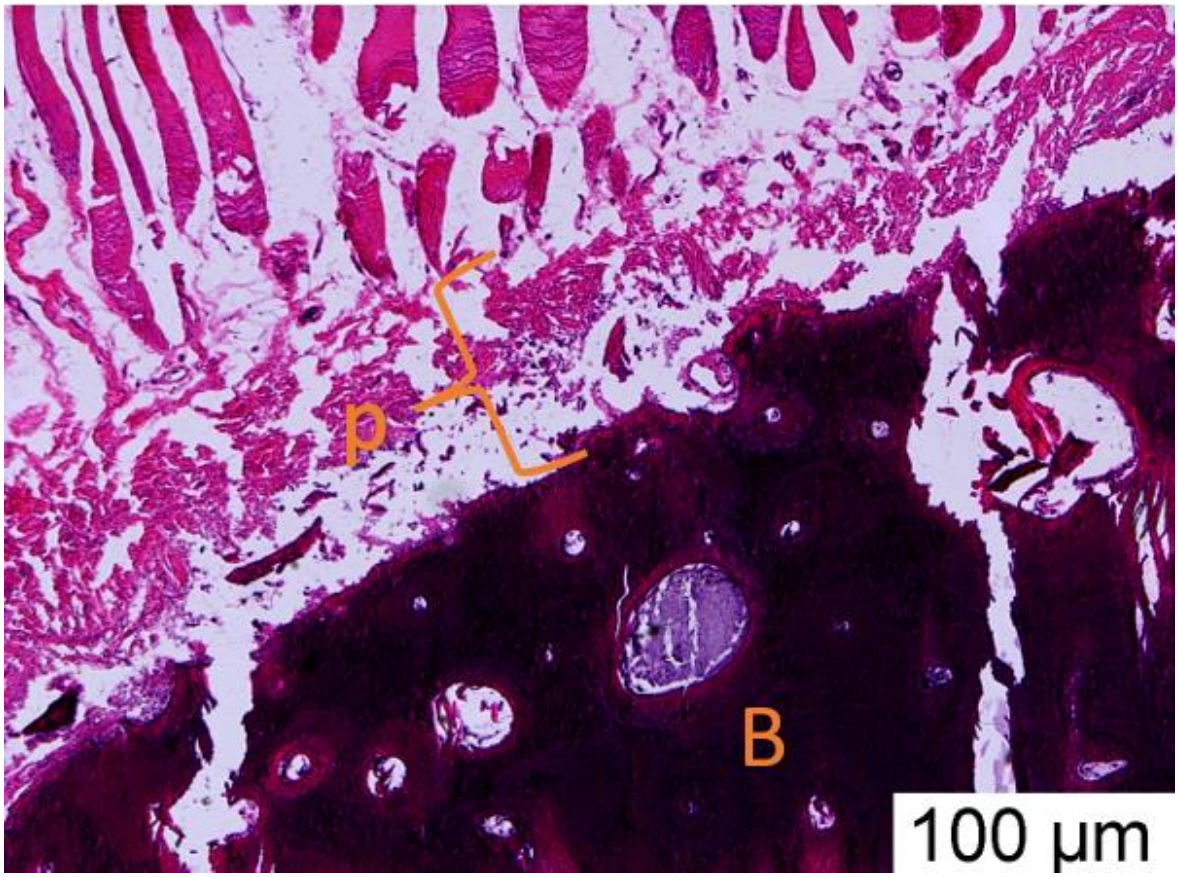

Image 1 shows intact human periosteum without any alteration in HE staining under light microscopy. In dark purple at the bottom, one can appreciate bone (B). Blood vessels, osteons and the haversian canal are visible in the bone. On top, the bone is covered by periosteum (P) which is then connected to muscle fibers and connective tissue.

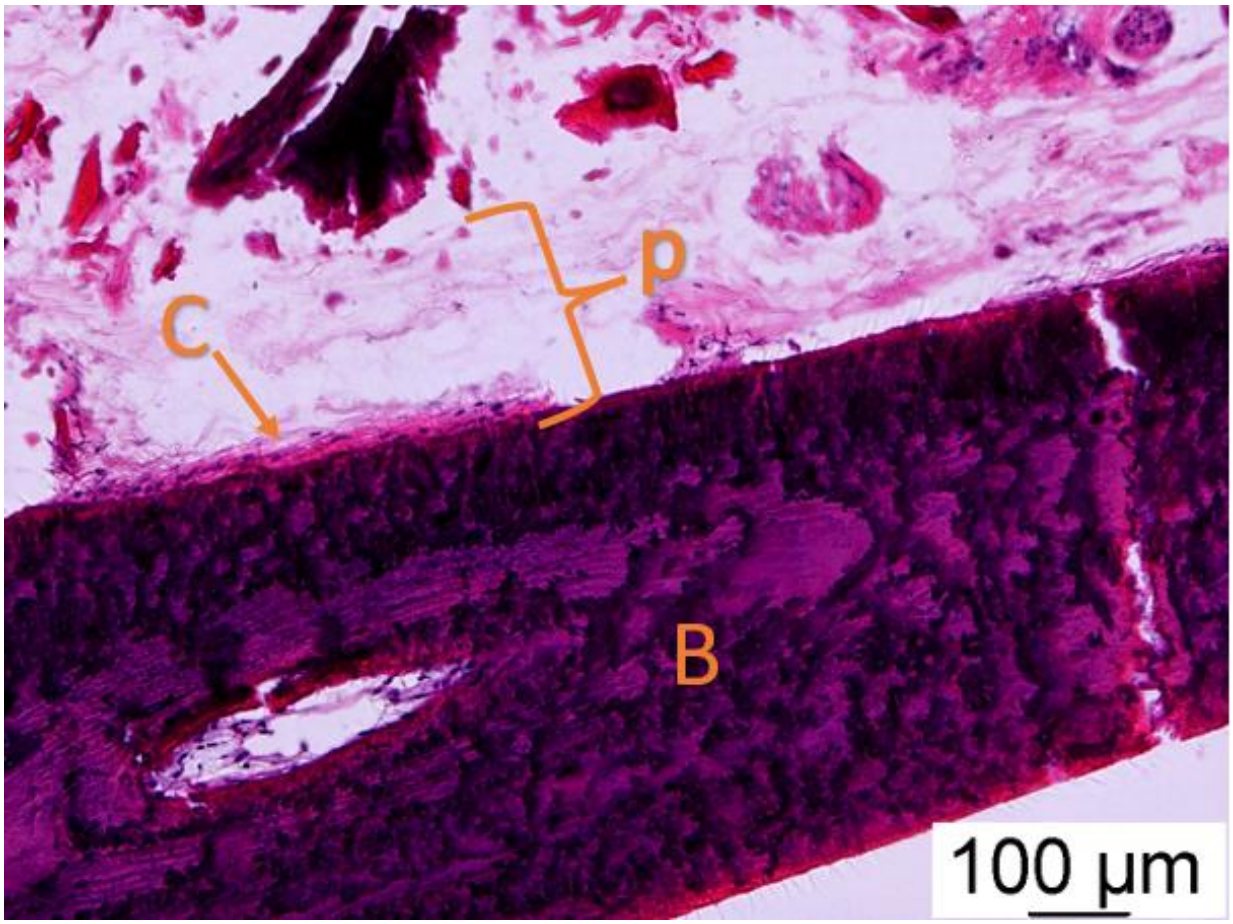

Image 2 shows intact human periosteum without any alteration in HE staining under light microscopy. In dark purple at the top, one can appreciate bone (B). Blood vessels run through the bone. On top of the bone part is the periosteal layer. Here, the cambium layer (C), with an abundant number of cells in close proximity of the bone, as well as the outer fibrous layer are visible. It is a very thin structure. Above the periosteum lies the connective tissue.

3.1.2 Histological analysis of activated periosteum after fracture

In case of a fracture, the periosteum activates, increases in size and becomes thicker in comparison to its inactivated status (see Figures 1 and 2). This can be seen in the histological findings as well. In the histological analysis of the activated periosteum, the cambium layer is visible and is distinguishable from the fibrous layer. An increased cellularity in the layers is also visible here.

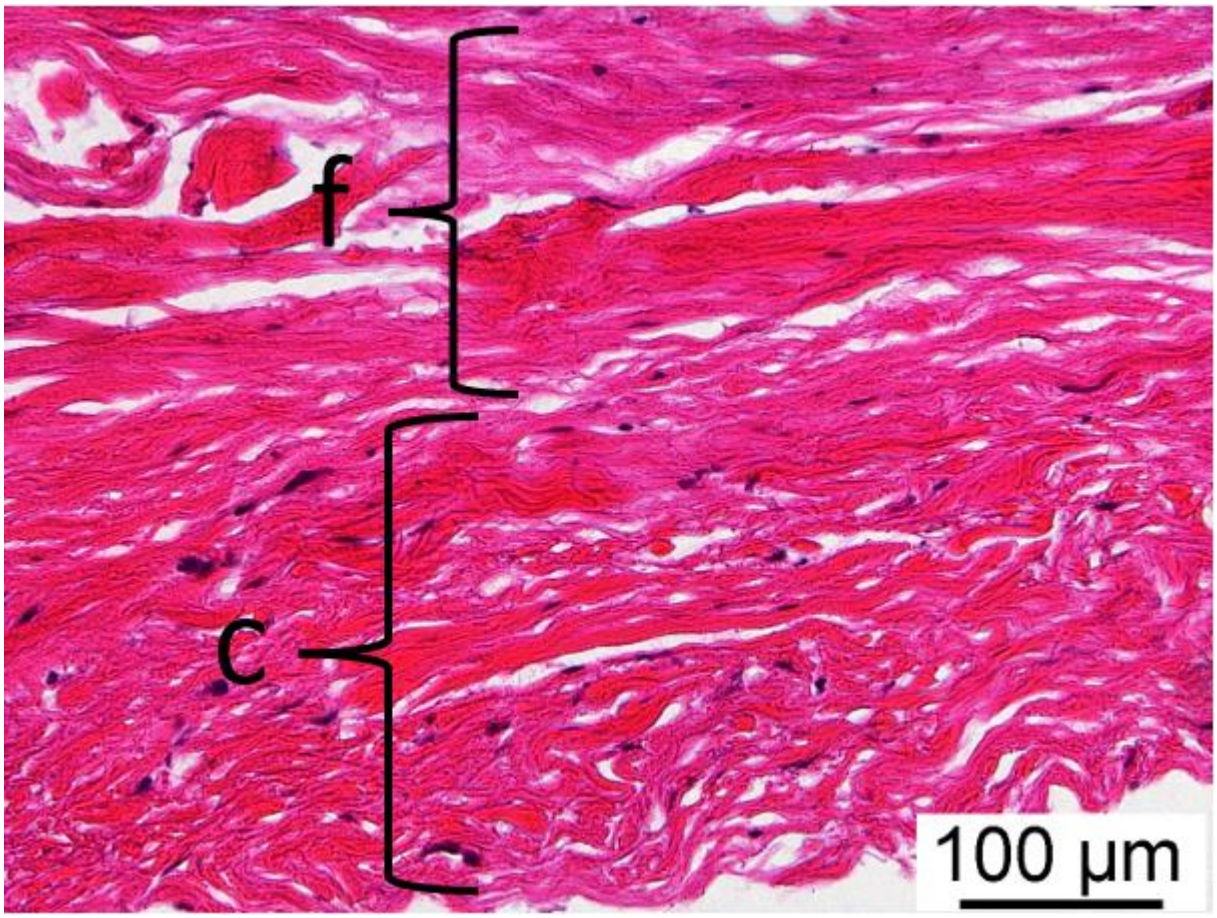

Image 3 shows activated human periosteum after fracture in HE-staining under light microscopy. An increased amount of cells is visible in the lower half the cambium layer (c) in comparison to the upper fibrous layer (f).

3.1.3 Histological analysis of the induced membrane

The induced membrane shows the two distinct layers. The inner layer closer to the spacer is thinner and presents with oriented cells, and without blood vessels. In contrast, the outer layer is further away from the spacer with many blood vessels and a lot of fibroblastic cells.

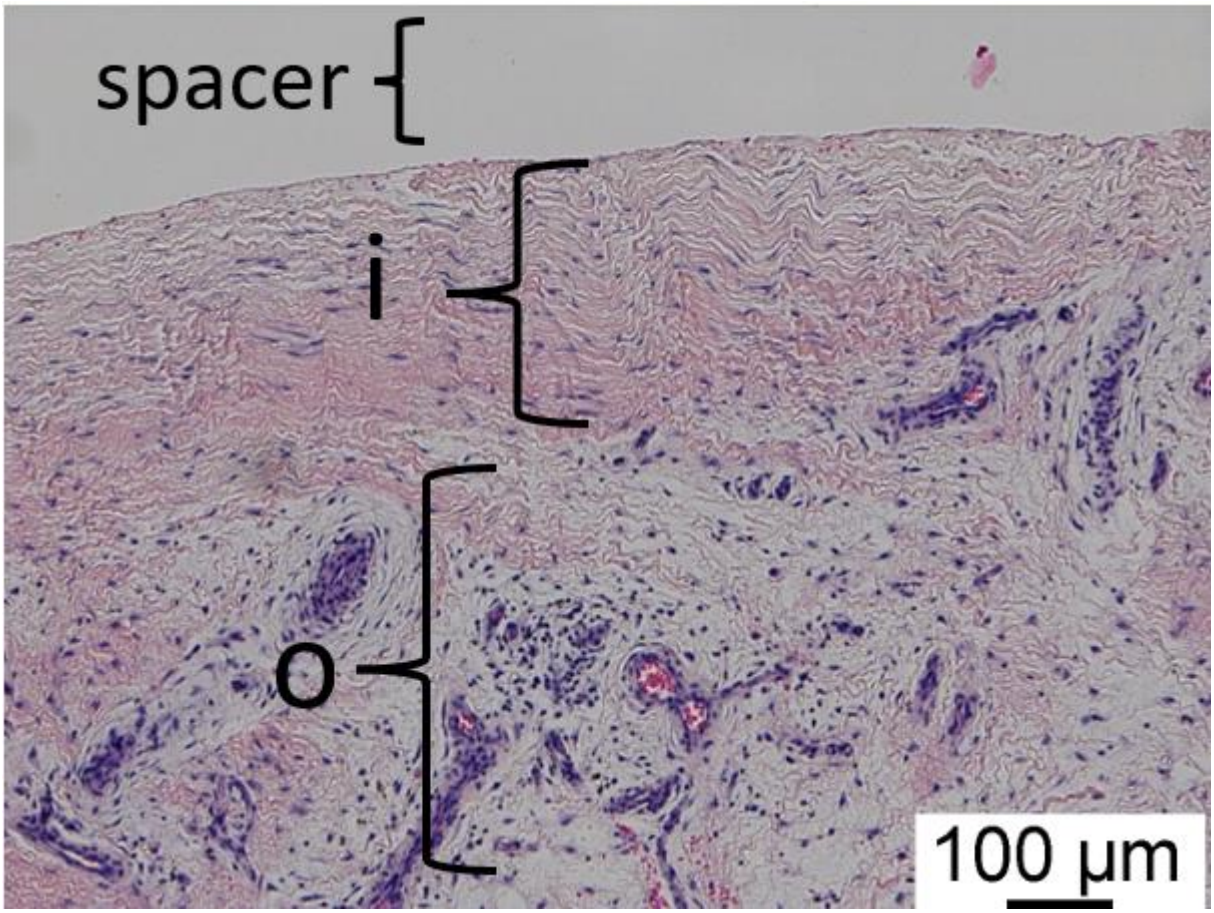

Image 4 shows induced membrane with inner zone (i) without blood vessels and thinner, oriented cells. Below is the outer layer (o), further away from the spacer (spacer) with blood vessels, fibroblast cells and fibrous extracellular matrix.

In the histological analysis of the induced membrane, the rich vascularity is visible.

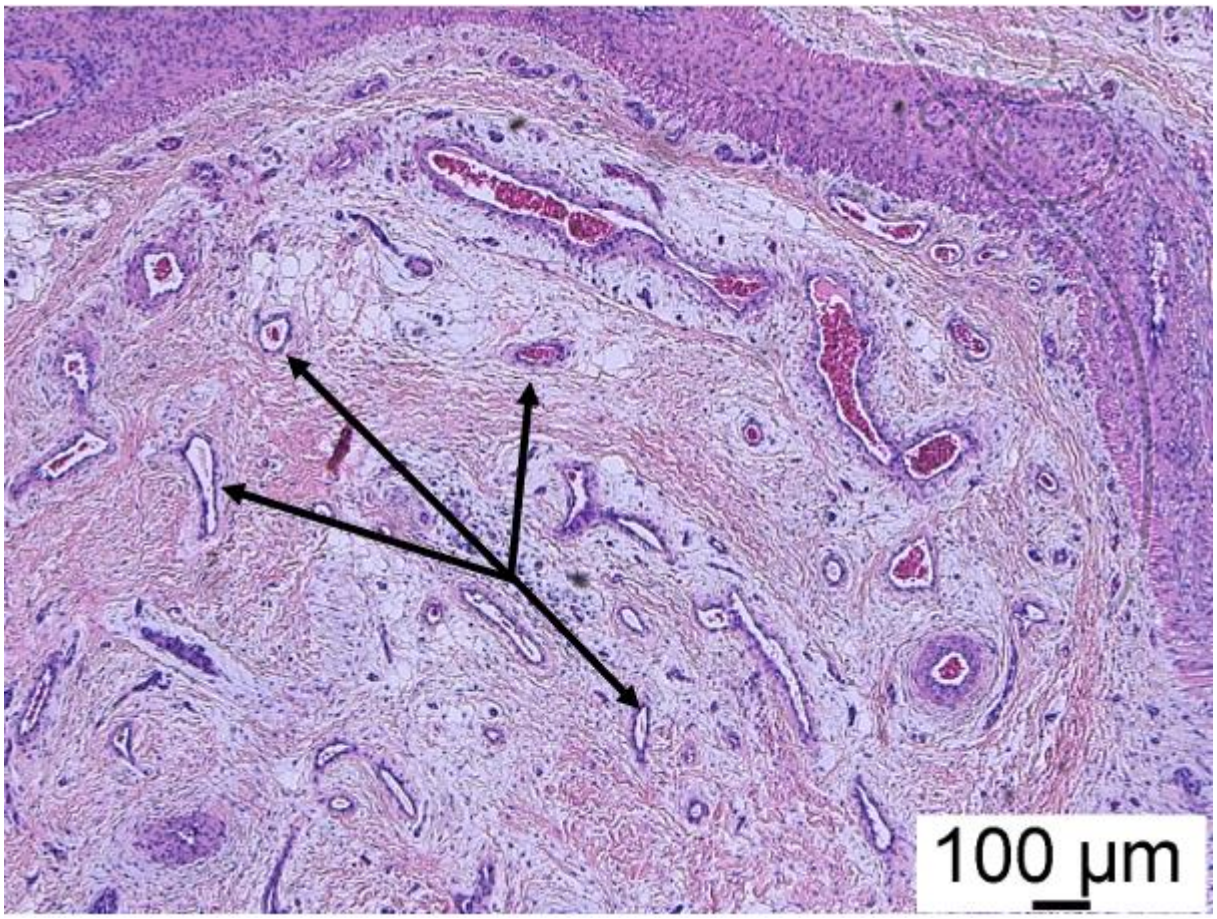

Image 5 shows induced membrane in HE staining under light microscopy. One can see the high vascularity of the membrane indicated by the arrows.

In addition, highly cellularised areas were visible within the induced membrane, hinting towards an ongoing inflammatory reaction process.

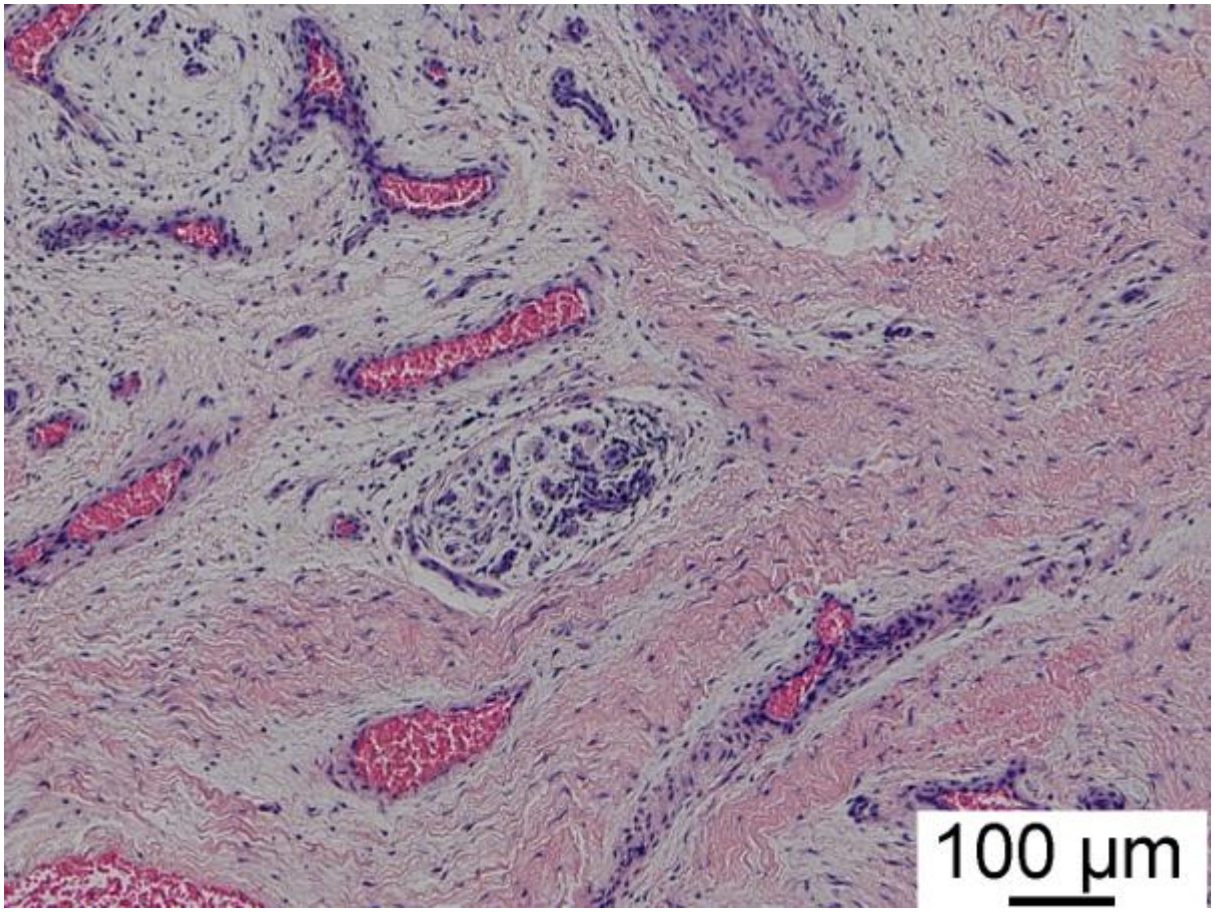

Image 6 shows induced membrane in HE staining under light microscopy. One can see the high cellularity of the membrane visible as blue stained nuclei everywhere.

The ongoing osteogenesis process is visible within the induced membrane.

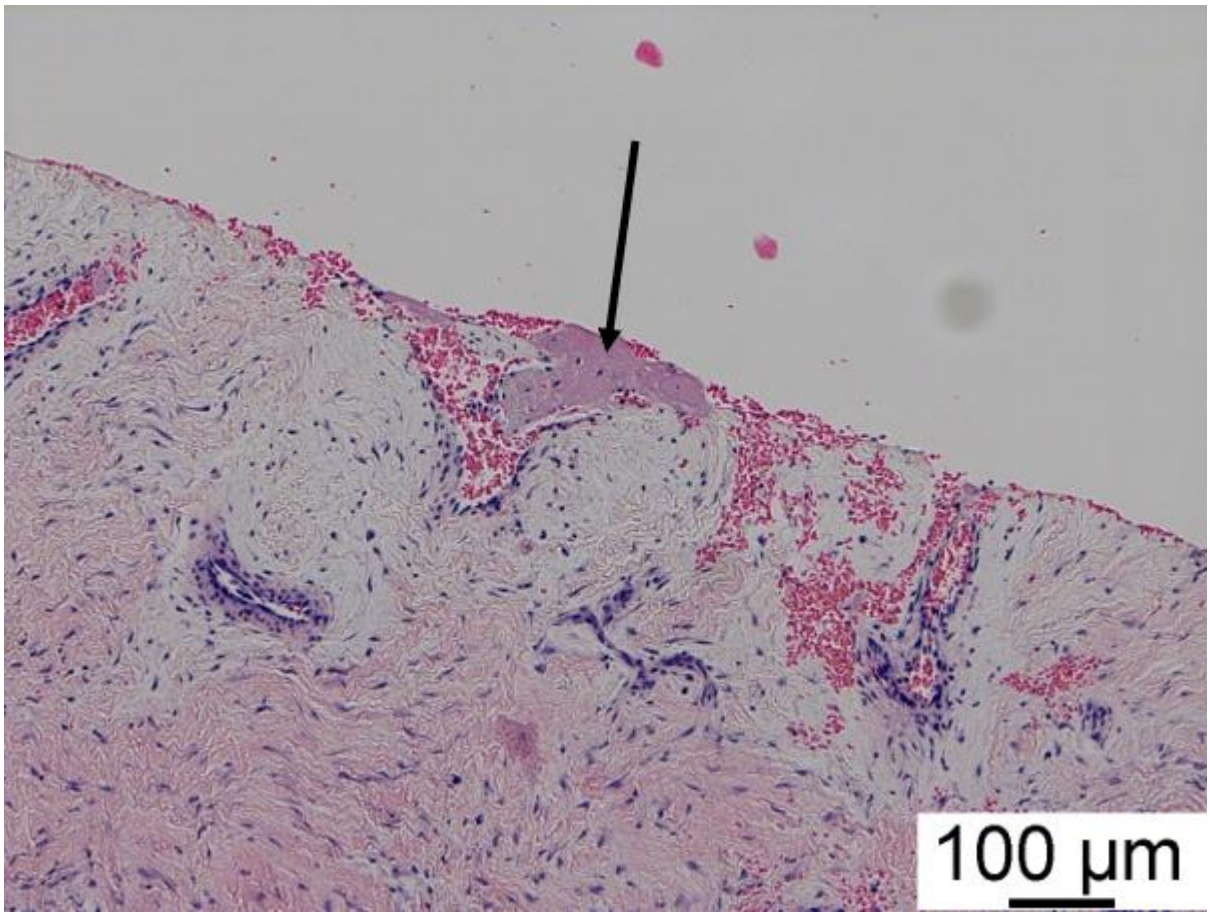

Image 7 shows induced membrane in HE staining under light microscopy. The ongoing osteogenesis in the membrane is visible (arrow).

Additionally, fat vacuoles are to be seen in the Masquelet membrane.

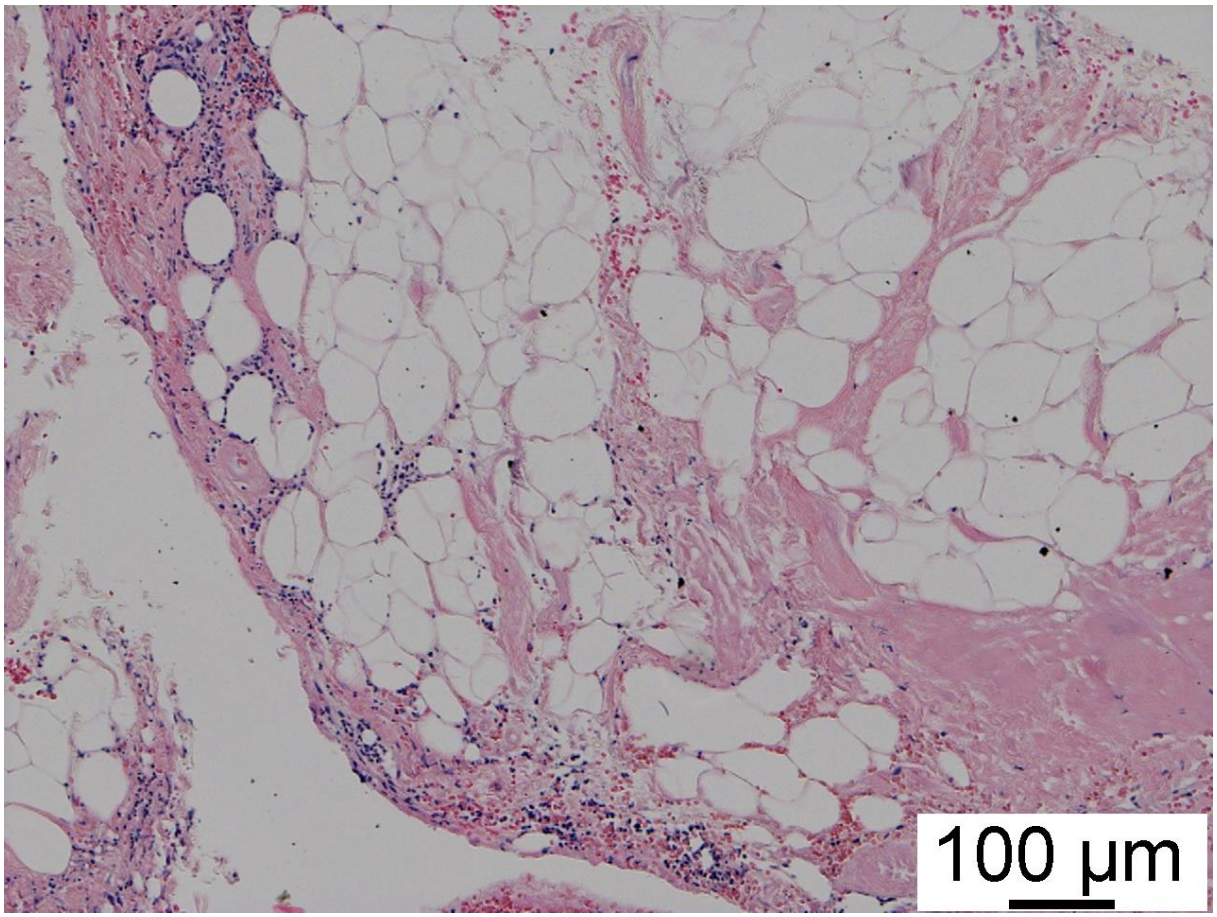

Image 8 shows induced membrane in HE staining under light microscopy. The fat cells are visible, with their large fat vacuoles that appear as empty bubbles with a very thin outer cell membrane.

The next image shows the same location of the induced membrane as image 4, but in Sirius red staining, which selectively highlights collagen fibers. Collagen represents the biggest component of the bone (89) and plays an integral part in its synthesis. In this histological picture, one can see the highlighted collagen fibers with increased abundancy closer to the spacer. Although there is a presence of these fibers ubiquitously, they accumulate in a high amount close to the spacer site.

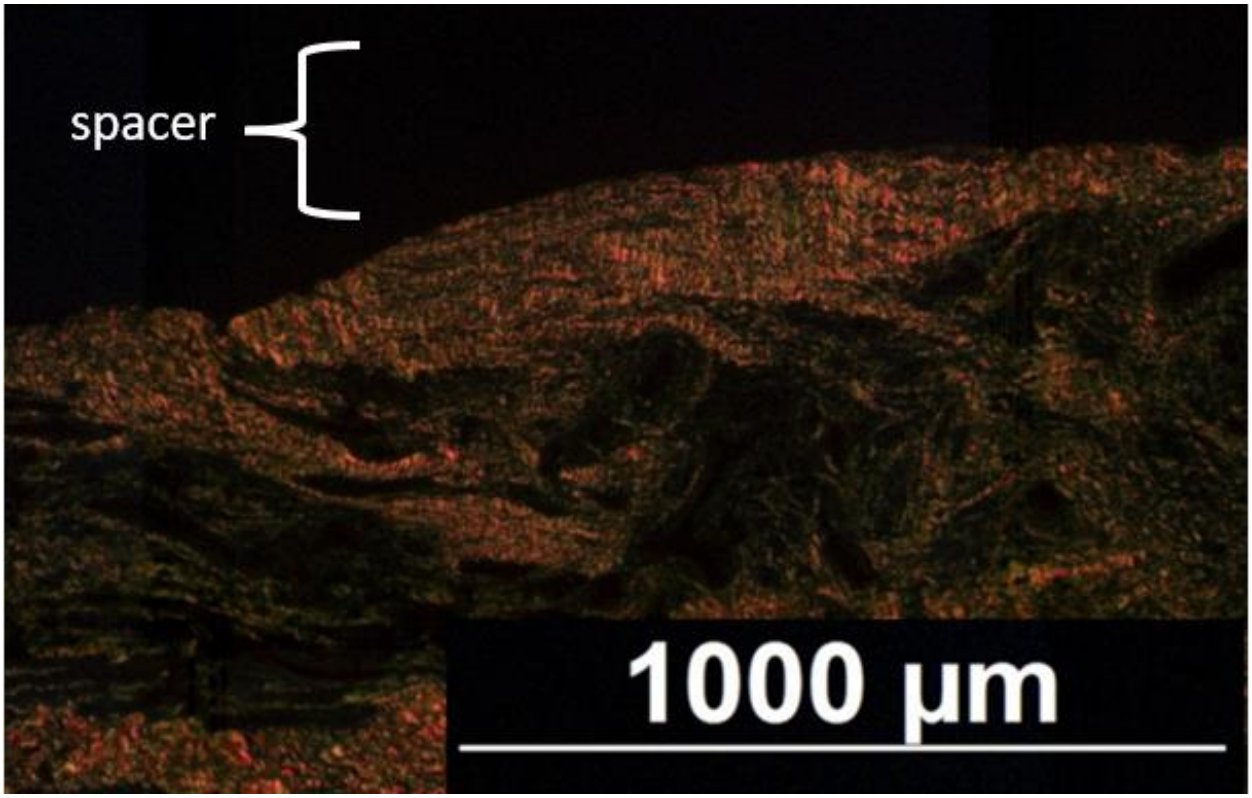

Image 9 shows induced membrane in Sirius red staining under light microscopy. One can see the collagen fibers lining the induced membrane at the site underneath the spacer.

3.2 Immunohistochemistry of vessel structures

The Immunohistochemistry of alpha-smooth muscle actin (α-SMA) shows the expression of myofibroblasts during wound healing (90). The myofibroblasts are involved in the tissue wound healing, especially in contraction and wound scarring (91). Additionally, α-SMA is also detected in pericytes, which are located in blood vessels, especially in the capillary system (92).

Images 10 and 11 show unaltered, intact periosteum. Here, only small amounts of α-SMA are detectable.

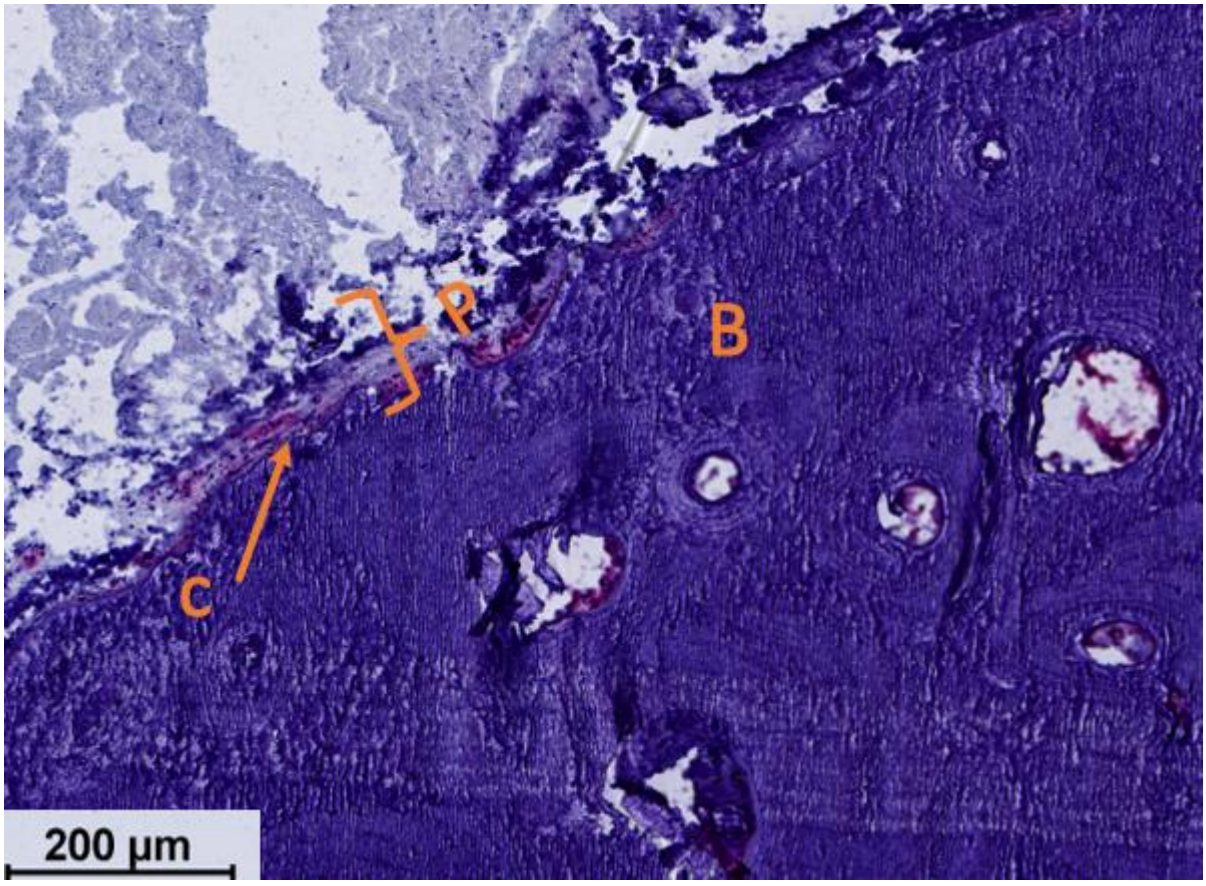

Image 10 shows unaltered periosteum via immunohistochemistry of α-SMA under light microscope. One can see the bone (b) as well as in light purple very little α-SMA expression in the cambium layer (c) of the periosteum (p). Some blood vessels within the bone show positive signals for α-SMA highlighting these blood vessels.

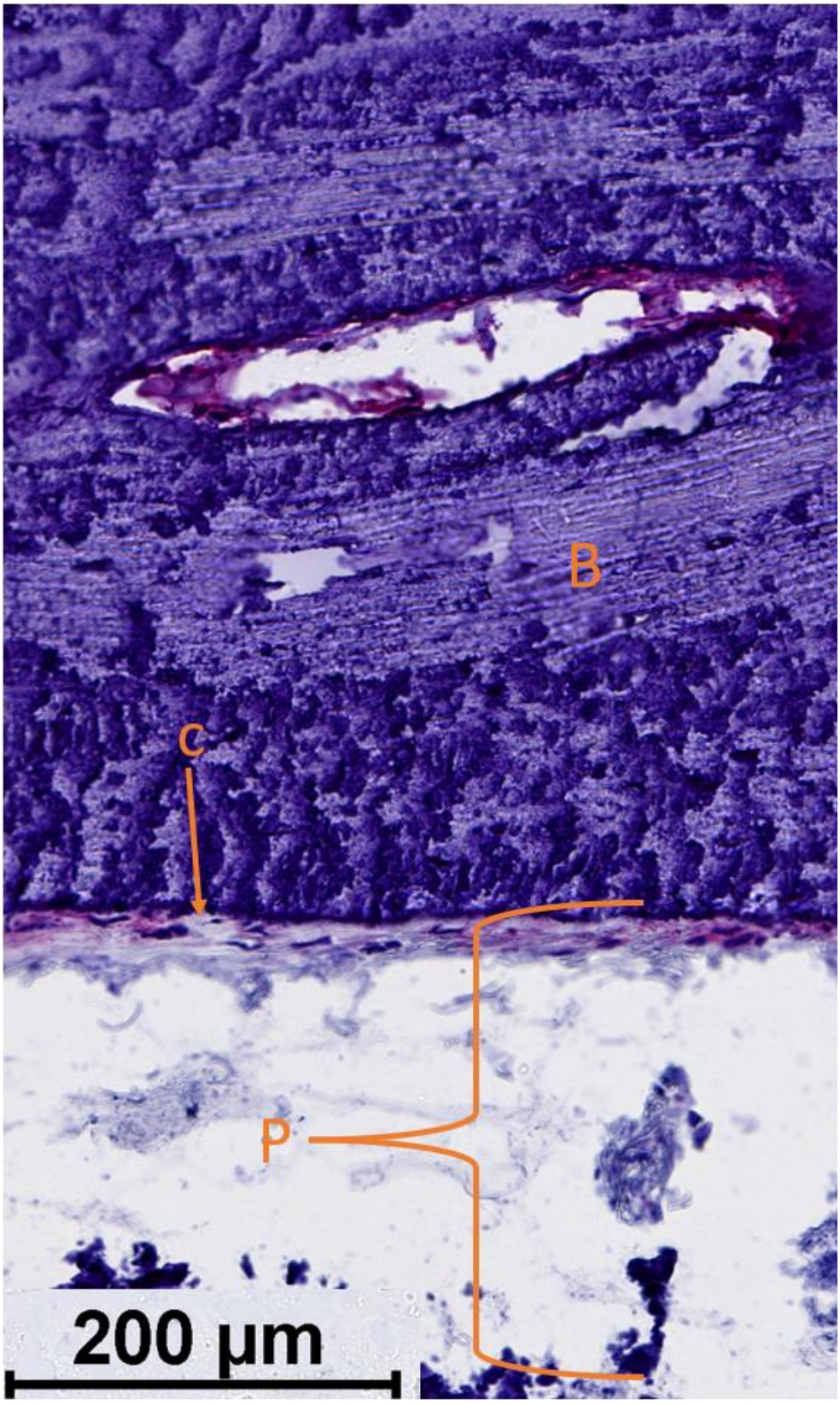

Image 11 shows unaltered periosteum via immunohistochemistry of α-SMA under light microscope. One can see the bone (b) as well as in light purple very little α-SMA expression in the cambium layer (c) of the periosteum (p). The present blood vessel within the bone shows positive signals for α-SMA highlighting this blood vessels even more.

Images 12 and 13 show periostea after fracture. Abundant α-SMA is visible as fibrotic changes are already ongoing, and not only surrounding the blood vessels but also within the periosteal tissue.

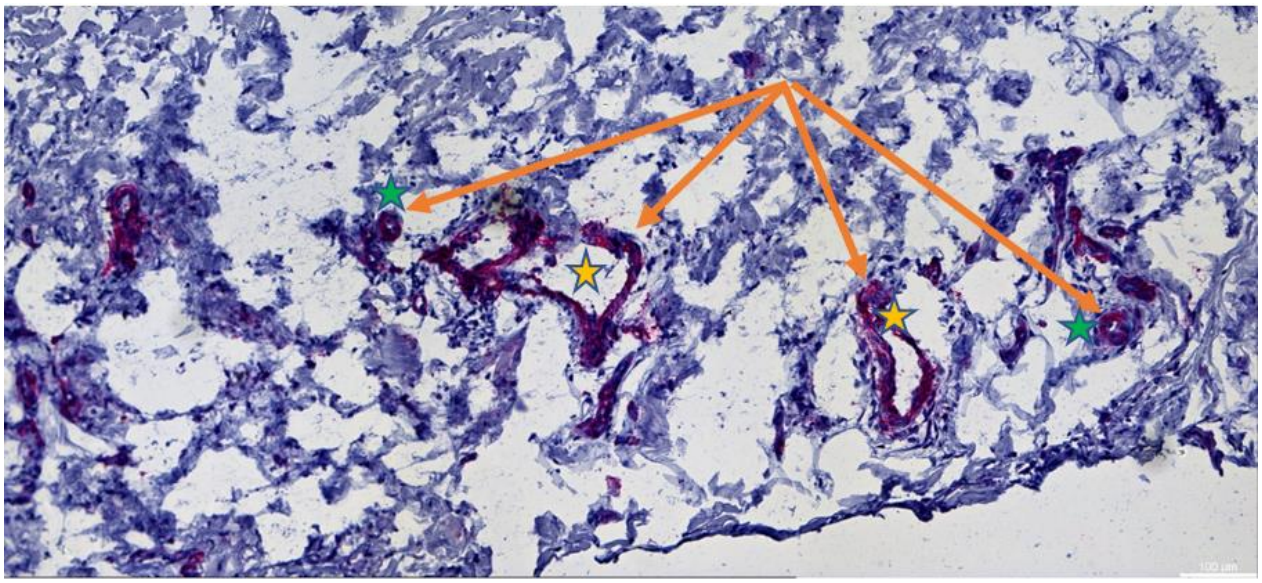

Image 12 shows activated periosteum after fracture via immunohistochemistry of α-SMA under light microscope. In light purple, the α-SMA expression is visible indicated by the arrows. Here, examples of arterioles (green star) and venules (yellow star) are indicated.

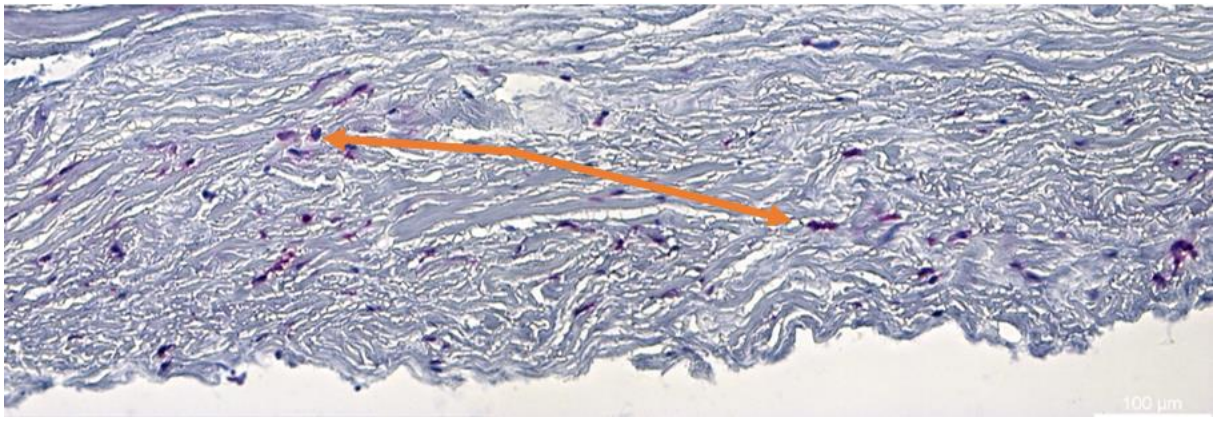

Image 13 shows activated periosteum after fracture via immunohistochemistry of α-SMA under light microscope. In light purple, the α-SMA expression is visible, indicated by the arrows.

In image 14, one can appreciate the abundancy of α-SMA expression within the induced membrane. As it is highly vascularized, many arterioles and venules are visible.

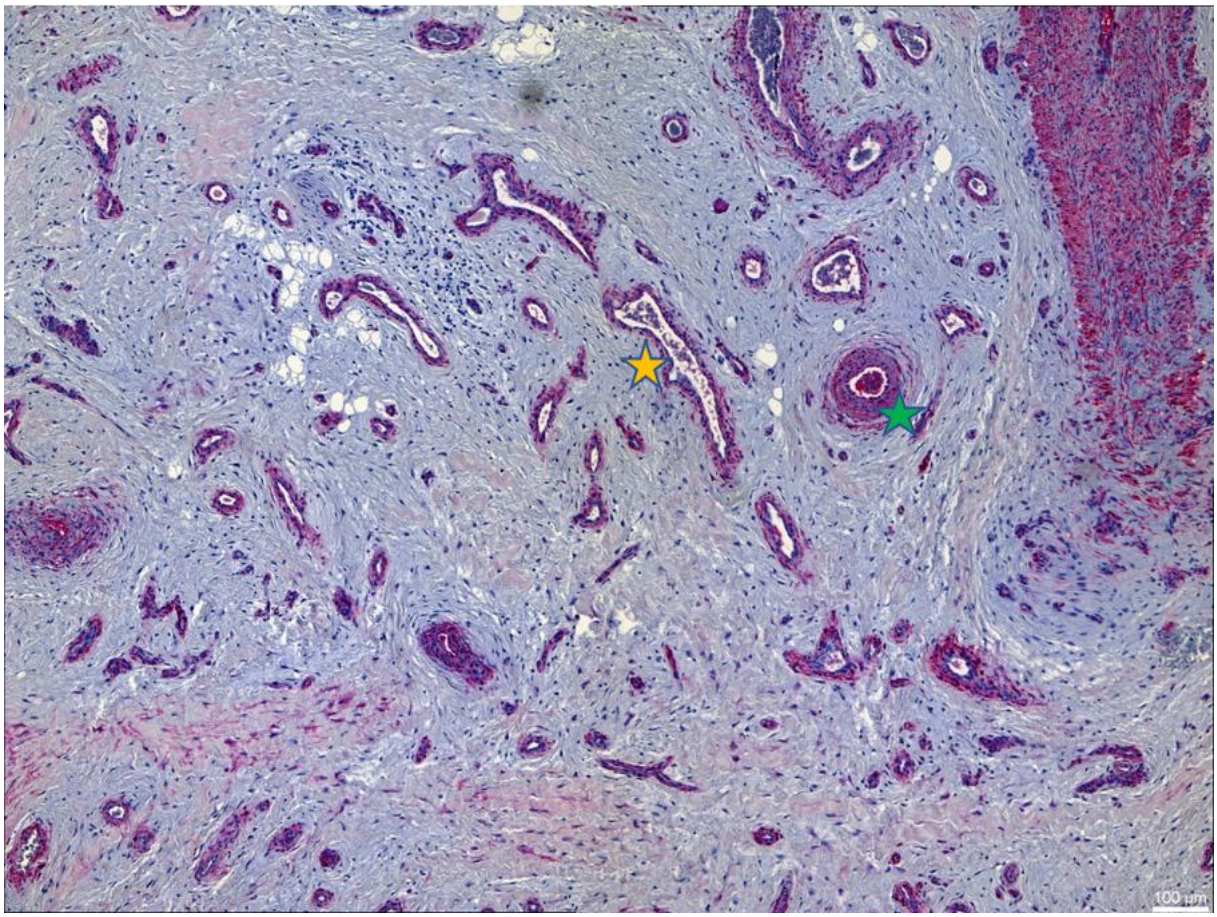

Image 14 shows induced membrane via immunohistochemistry of α-SMA under light microscope. In light purple, the α-SMA expression is visible. One can appreciate the abundancy of blood vessels and associated expressions of α-SMA. Here, examples of arterioles (green star) and venules (yellow star) are indicated.

3.3 Expression analysis

The RT-qPCR expression analysis shows the comparison of inactive periosteum, activated periosteum and induced membrane regarding the targets of interest.

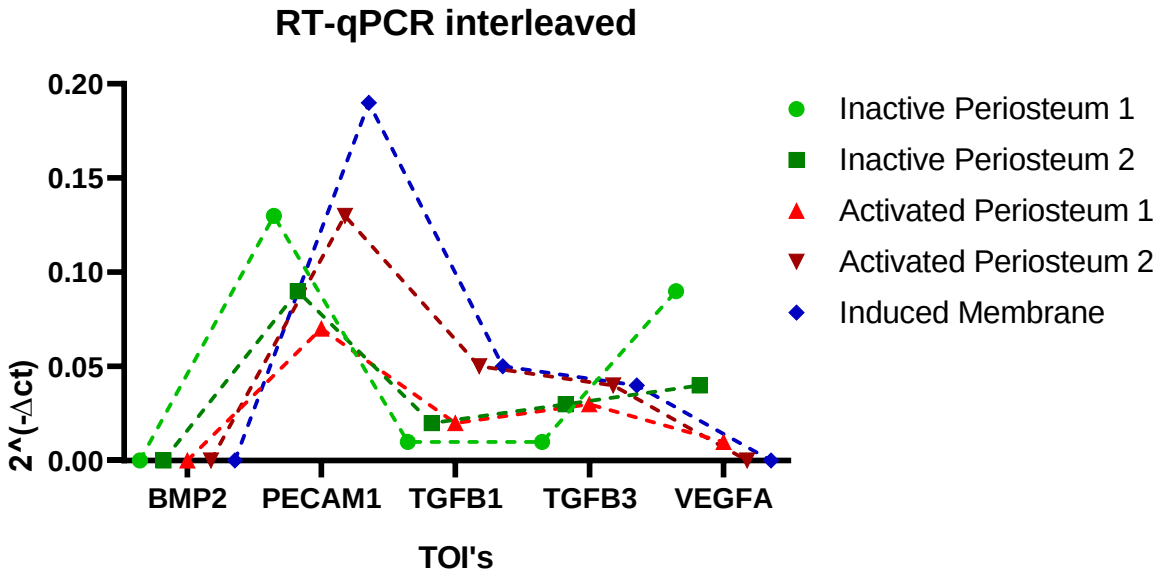

Figure 5 shows the RT-qPCR results of the two inactive periosteal samples in green, the two activated periosteal samples in red and the induced membrane in blue. The dotted lines are merely for better visualization of the results.

The expression analysis shows that there is no expression of BMP-2 in all samples, and there is high expression of PECAM-1 in both inactivated and activated periosteum, but that the induced membrane expresses notably more. TGFβ-1 shows a higher expression in the activated periosteum as well as in the induced membrane in contrast to the inactivated periosteum. TGFβ-3 shows comparable results. VEGFA is primarily expressed in the activated periosteum, to a lesser or no extent in the activated membrane, and not at all in the induced membrane. It is noticeable that the induced membrane as well as an activated periosteum sample in TGFβ-1, TGFβ-3 and VEGFA show very similar expressions, and in PECAM-1 a similar positive deflection.

4. Discussion

4.1 Discussion of retrospective analysis about non-unions

The retrospective analysis documents that 325 surgeries were performed under the code M84, which stands for continuity of bone, and among them, 209 cases were further subdivided as M84.1 – Non-union of fracture (Pseudarthrosis). Thus, 116 patients were registered under a different ICD-10 code. An alternative is M84.2 - Delayed union of fracture, which develops into non-union after three months without evidence of healing (20), is diagnosed earlier, and therefore could still develop into a non-union of fracture. While the distinction is very clear by definition, it may not be applied with quite as much accuracy in clinical practice. This could result in an inappropriate classification, as the two pathologies are not only very similar, but also directly related. Therefore, M84.1 could have been diagnosed even though it was M84.0, and vice versa.

According to the statistical data from "Destatis", there were 70,005 cases of M84 in Germany in 2017-2019, of which 38,527 were more precisely documented as M84.1. In Berlin, there were 3,300 diagnoses of M84 in these three years. The Charité Campus Virchow clinic diagnosed 325 cases of M84, of which 209 were M84.1 diagnoses. This concludes statistically for every 2,154 inhabitants in Germany, one M84.1 is diagnosed and in addition, for every 1,185, the M84 diagnoses is given.

This agrees with the figures for Berlin, where there is one M84 diagnosis for every 1,090 inhabitants. This shows that the results of the retrospective study can be considered representative of the situation in the Federal Republic of Germany. From the statistics presented, it is clear that there exists a relatively frequent clinical need for the treatment of non-union pathologies, and that it is therefore important to be aware of the available treatment options. In total, the induced membrane technique was successfully applied six times in the Charité Campus Virchow clinic over the three years. For this healing method, the outcome of the therapy was elicited. For further analysis, it would be interesting to study the other applied techniques and look into their healing results, which were applied during the course of the three years.

4.2 Morphological resemblance between the induced membrane and the periosteum

Part of the work conducted was intended to highlight the influence of the periosteum on bone healing. Therefore, a comparison was made between inactive periosteum in the physiological state, the activated periosteum after fracture, and the induced membrane regarding their composition and cellular activity. There are several difficulties in obtaining the samples, especially activated periosteum and induced membrane. First, only the material that is routinely discarded and not left in the body to heal can be used - additional material cannot be removed. The importance and influence of the periosteum in fracture healing has been thoroughly described. Second, the periosteum and the induced membrane are so battered, rolled up and crushed into each other that exact anatomical orientation is no longer possible during harvesting and especially later.

Easy orientation is possible in the inactivated periosteum, since the bone is also removed during the operation and thus exact anatomical positions are clearly visible. In the inactivated, unaltered periosteum, the different layers are barely visible as they are very thin and in a quiescent status. The cambium layer, which is the inner membrane closest to the bone, has a higher amount of cells than the fibrous layer, further away from the bone. The latter layer is subdivided as well, into the fibroblastic layer and superficial layer. The fibroblastic layer contains fibroblastic cells, whereas in the superficial are layer, there are loose collagen matrix, and the majority of blood vessels are located in the periosteum. Despite the idle status of the periosteal layer, the different cellular components as described are appreciable. Despite the aforementioned difficulties of allocation, these layers are easier to be differentiated in the activated periosteum as they grow and become active. In particular, the cambium layer is markedly bigger in size, and has more cells. These cells have a high proliferation rate and retain their potential differentiation capacity, as they are able to differentiate into skeletal myocytes, adipocytes, chondrocytes, osteoblasts and fibroblasts (29). The thickness of the membranes differ in inactive periosteum, activated periosteum and induced membrane (44).

Similarly to the activated periosteum, accurate anatomical orientation in the induced membrane is more difficult. However, the two distinct layers were visible and distinguishable, findings which were reported by other authors as well (71). The layer closer to the PMMA spacer appears without blood vessels and in an oriented fashion,

with less cells than in the layer which is further away. Here, there are many blood vessels to be seen, as well as many periosteal cells. The blood vessels in the layer further away from the PMMA spacer are abundantly visible. The increased amount of blood vessels is also reported in the literature, and even unconstrained by the time frame of the second surgery (72). Additionally, an ongoing ossification process is visible depicted in Image 7. Other authors have reported similar findings of an ongoing endochondral ossification process in their samples, like Niikura et al., who hypothesized that it might be due to a cause-and-effect mechanism, as “rich vascularity may induce bone formation inside the induced membrane” (72). Furthermore, the appearance of collagen in the induced membrane is visible in Image 9 and is also reported by other authors (93). Collagen matrix is mineralized and used for the synthesis of bone (89), hence its availability in the fracture repair mechanism is of high importance.

Additionally, fat vacuoles are to be seen in the Masquelet membrane. This has already been described by other authors (13). Since the fibroblast lineage can express either osteoblast-like or adipocyte-like markers, it reinforces the theory that multi-potent mesenchymal cells build fat vacuoles, and further indicates the close relationship between fat metabolism and bone metabolism (94).

4.2.1 Mirror-inverted arrangement of periosteum and induced membrane

The arrangement of the two different periosteal layers in proximity to the bone is the cambium and the fibrous layer, respectively, but the arrangement of the two layers appears to differ in case of the induced membrane. Although the histological images were like those of other authors (95), who have also described this structure, the mirror-inverted arrangement of periosteum and induced membrane has not been explicitly mentioned or described by other authors. In the undamaged periosteum, the cambium layer near the bone has a high cellularity but is relatively thin, and the fibrous layer far from the bone has fewer cells and more fibrous connective tissue, as can also be seen in the histological images. The same applies in the case of the activated periosteum. Despite the difference in size of the membranes, as they are thicker in case of activated, altered periosteum, the arrangement is the same. Interestingly, the arrangement in the induced membrane is

mirror inverted. The high cellular layer, which is also thicker and has a lot of blood vessels, is located further away from the spacer than the fibrous connective layer.
This inversion is possibly caused by direct contact with the spacer and the associated inflammatory reaction, with fibrous changes that form around the spacer due to the foreign body reaction, enclosing it like a capsule.
The fibrous changes occurring in the activated periosteum in comparison to the unaltered periosteum are also visualized in the immunohistochemistry, as α-SMA is abundantly expressed. In addition to the occurrence in the blood vessel network, it is also visible ubiquitously. In the unaltered periosteum, some expressions are to be seen in the cambium layer of the periosteum. This is probably due to the angio- and vasculogenesis functions the periosteum is involved in.

4.3 Resemblance of cellular expression between the induced membrane and the periosteum

The RT-qPCR indicates whether genes of certain cells are expressed and in what relative quantity. To evaluate the angiogenic and osteogenic potential of the induced membrane, inactive periosteum, and active periosteum, I selected the following target genes for analysis. To assess the angiogenic processes taking place, I chose PECAM-1, because it is a marker for a signaling molecule involved in angiogenesis (96), and VEGFA, which is a marker for angio- and vasculogenesis (13). Adequate vascularization and blood supply are essential for bone growth and fracture repair, as I explained before. For the analysis of fibrotic processes taking place, I chose TGFβ-1, because it is a marker for the regulation of differentiation and cell growth (97), and TGFβ-3, which is a marker for the production of extracellular matrix (98). Both are used to analyze the allegedly scar-like structure that forms around the foreign body. For the analysis of the osteogenic processes taking place, I chose BMP-2, because it is a marker for bone and cartilage growth (37).
In the case of inactivated periosteum, the expression of TGFβ-1 and TGFβ-3 are lower, and in the case of VEGFA higher than the expressions of the activated periosteum and induced membrane. Only VEGFA is higher expressed in inactivated periosteum, possibly because the periosteum continuously establishes further blood supply, expanding from pre-existing ones and building entirely new capillaries and blood vessels. However, in

case of fracture, the blood vessels and capillaries are already built, but not intact anymore, resulting in the higher expression of PECAM-1 as it is marker for angiogenesis. This promotes a vascular growth focused on reestablishing connections rather than creating new blood vessels.

In the case of the induced membrane and the activated periosteum, they are most similar in the expression of the TOI's chosen here, indicating the functional similarities of these two tissue types and that the induced membrane acts somewhat like an activated periosteum. In both PECAM-1 and TGFβ-1 as well as in TGFβ-3 the expressions are similarly high, whereas the same similarities for the induced membrane and the activated periosteum are found in VEGFA and BMP-2, but with lower expression. For the expression of genes, the time of harvesting naturally plays a major role with regard to the ongoing fracture healing process. As I have already explained and described, the different phases of bone healing are not clear cut, but rather a transition into the respective phases. The inflammatory reaction which occurs initially after a fracture is already finely balanced, and within this phase, a shift from early proinflammatory reaction to a suppression of inflammatory reaction occurs (14). Regarding the removal of the activated periosteum, it was, of course, removed as far as the clinical setting allowed it, without any scientific considerations during the surgery. Therefore, the periosteum may have been removed in a phase in which certain cellular processes may have either already ended or not yet begun. Bearing that in mind, it is also noticeable that neither the inactivated periosteum nor the activated periosteum, and above all not even the induced membrane, expresses BMP-2. This cannot be confirmed in the literature, where BMP-2 is described as a highly expressed macromolecule (65). The lack of expressed genes of this protein can have different reasons; on the one hand, the work could have been unclean, but the no-reverse transcription control (NTC) was always negative, and there was no contamination of the samples. Another theory is that the provided primer could be faulty, and therefore not show BMP2 expression. However, subsequent testing disproved this theory. Assuming that there is no error in the RT-qPCR and that BMP-2 is in fact not expressed, this would lead to a rethinking of the importance of BMP-2. How can there be no BMP-2 expression if an ongoing ossification process is already visible in the histological staining, as a missing BMP-2 annuls the callus formation (29)? It is possible that the BMP-2 is expressed only at a certain time or stage of healing, and it was not expressed anymore when I measured it. Furthermore, the low number of both periosteal tissue samples (n=2)

and induced membrane (n=1) presents a limiting factor in providing extensive comparability for the findings. Research conducted with a higher amount of samples could provide enlightenment.

According to Prof. P. Giannoudis, several open questions about the induced membrane remain unanswered. In his PowerPoint presentation (8.7.2021 Wolff Lecture of the SFB 1444 digitally – due to Covid), he mentions uncertainties about the gross morphology of the induced membrane, which cytokines are present, what the cellular constitution is, the tri-lineage potential of the cells present in the induced membrane, and the pattern of gene expression. Furthermore, he questions the comparison of these points with the periosteum, and whether the membrane is actively involved in the formation of new bone. In this work, for example, I have been able to show the different morphological features of the induced membrane, like the presence of blood vessels or ongoing ossification processes, whereas on cellular level I have been able to compare the expression of genes which are involved angiogenesis and vasculogenesis.

4.4 From a two stage to a one stage surgery of the induced membrane

Smaller defects with a size of up to 4 centimeters can be treated with an autologous bone transplant, whereas larger critical size defects require even more complex reconstructions and surgeries (99). The two surgical techniques in the treatment of CSD that are mainly focused on in this work are segmental bone transport and the induced membrane technique. The Constant improvements led from the initial segment transport by Ilizarov to today's mechanical nail transport, which has been extended even further by electric nail transport and magnetic nail transport (55). These refinements to the original technique lead to a significantly increased quality of life for the patients. The remaining disadvantages of this technique are pin-tract infections or joint stiffness, which require further investigations to further improve the technique (52). The advances in treatment techniques might account for the low numbers of induced membrane treatments within the Charité Campus Virchow clinic.

Although many improvements in intramedullary nail transport are taking place and have taken place, and even though the induced membrane technique is currently a two-stage operation, with all its disadvantages, this technique presents an alternative surgical

option. The induced membrane is already proven as a universally applicable treatment method, despite aforementioned limitations (75). Regardless of the fact that the induced membrane technique has not yet overcome the main problem of being two-stage surgery, there are already many approaches and ideas for its conversion into a one-time surgery. Via imaging techniques like computed tomography, magnetic resonance imaging or computer aided design (CAD), the injured site can be visualized, and models for electrospinning and 3D printed scaffolds can be created accordingly (100). This allows direct control of microarchitecture and anatomical structure to fit perfectly for each patient's defect site (59). These scaffolds have to meet certain requirements to work efficiently - they have to be biodegradable, support osteogenesis, while providing osteoconductivity, and osteoinductivity while still being biocompatible (101). The material polycaprolactone, for example provides good viscoelasticity and is biodegradable, and thus it presents as a beneficial scaffold material for bone tissue engineering (59). These scaffolds can involve granules inside them, and the size of the granules has many influences on the surface-to-volume ratio, on the 3D structure, on the immigration of nutrients, cells, and blood vessels, on the mechanical stability and on material dissolution and resorption characteristics. Variations in granule size will result in different expressions of these conditions (102). Artificial development of the biological membrane which develops during the first stage would save the patient the second operation and improve quality of life immensely (99). Before the establishment of a single-stage induced membrane technique and its application to humans, animal experiments with this membrane would be first necessary to ensure the aforementioned properties.

Generally, it is indispensable that the treating physicians have exact knowledge of the clinical situation that is presented. This includes not only the severity of the injury, but also comorbidities and other patient related factors, what treatment strategies are necessary, and what methods may still need to be used to allow the patient to recover, to only mention a few aspects that have to be considered in the successful treatment of the patients (103).

At this point in time, there is no universal gold standard in the treatment of CSD, but it is a matter of weighing the respective advantages and disadvantages in the respective situation against the given possibilities and specialists' skills. In this respect, the treatment method that promises the greatest healing success in the specific situation should be selected (104). The continuous research and scientific evaluation of these techniques are

of great importance for the improvement of patient care. Therefore, from a clinical point of view, converting the two-stage procedure into a one-stage treatment procedure would be of great interest for treatment. Therefore, in the present study, an attempt was made to find the correspondences between the spontaneous healing process of a fracture by the periosteum and the evoked healing process by the induced membrane, as the induced membrane around the cement block resembles the periosteum in anatomical and histological structure as well as cellular composition (105). Both the periosteum after the fracture, which is directly involved in the healing processes, and the periosteum in the physiological state were analyzed and these results were compared with the induced membrane technique. Hence, these three tissue types were chosen for analysis.

4.5 Limitations

The conducting of scientific studies on human beings is, of course, always subordinated to the well-being of the patients. Therefore, it is necessary to complement the results of animal studies with research with human specimens, because quantitatively, the extraction of material is subject to the ethical requirements of prioritizing the prospects of cure of the injured patient.

Hence, a limitation of this work is the small number of periosteal tissue samples (n=2) and induced membrane (n=1), which prevents comprehensive comparability of the results. Studies performed with a larger number of samples may provide insight in this regard. In addition, the activated periosteum is damaged after a fracture and rolled up. Normally, only damaged periosteum which overlies the wound margin of the fractured bone is discarded, while the remaining periosteum is used for bone healing. Therefore, the specimen acquisition depends on how far the fracture has damaged the periosteum, how far the periosteum remains in the body for healing, and how much is discarded. Furthermore, there is also damage to the musculature and connective tissue, which cannot be differentiated intraoperatively and afterwards. Additionally, the specimen material is not always taken at a specific time and distance from the present injury. Therefore, the tissue conditions exhibit different stages of healing. Additionally, the timing of the sample transfer and the insertion into the respective medium or freezing is dependent on the ongoing operation. All these factors alter the results, which is further

complicated by the periosteum being a very fragile and thin tissue and thus one needs a lot of it for analysis.

4.6 Further investigative methods and contributions to medical sciences

Clinically applied examinations of the bone healing process can also provide further information. For example, computed tomography scan, magnetic resonance imaging (with contrast medium, without contrast medium) positron emission tomography, or ultrasound can provide non-invasive evidence of healing processes taking place. Furthermore, tissue samples can be analyzed, similarly to this study. The results of light microscopy could then be compared with the results of transmission electron microscopy or scanning microscopy, as well as different immunohistochemical or radioactive labeling strategies could be applied.

The single-stage procedure is already being used in animal studies. If the procedure is then also applied in humans, the present study could allow for the comparison of the healing processes of the artificially produced induced membrane from the 3D printer with the healing processes of the induced membrane produced by the cement spacer and the healing processes of the periosteum. The present work could provide a small contribution to further adaptations, modifications and improvements of the induced membrane technique in the context of clinical application.

5. Conclusion

Critical size defects remain a significant challenge for both the patient and the treating team. To date, the reconstruction of these defects represents a significant socioeconomic burden. Due to the variable etiology, preventative approaches for CSDs are not possible. Hence, optimal treatment supporting the regrowth of the lost bone is essential in reducing morbidity and invalidity.

The periosteum plays a significant role in skeletal regeneration, as it provides the foundation of the signaling pathways for vasculogenesis, angiogenesis and bone formation. In a CSD, a biological stimulus must be supplied to aid regeneration. Bridging the gap may be achieved by bone transport techniques or bone grafting while optimizing osteoconductive and osteoinductive properties.

The induced membrane technique provides a biological environment that mimics, in a mirror-inverted arrangement, the function of an activated periosteum, and provides the bioreactor required for bone healing. Additionally, the induced membrane provides osteoinductive, osteoconductive and osteointegrative functions. Several factors complicate the surgical treatment of CSD, like the limited availability of bone graft or patient-related factors and morbidity. To overcome these hindrances, other materials that provide additional osteoconductive or osteoinductive properties can be applied (65).

The disadvantages of bone grafting can be alleviated by combining it with Masquelet's technique.

Additionally, the induced membrane technique is a reliable solution in the treatment cascade of CSDs. As highlighted, the advantages of the Masquelet's technique are its good healing results, with manageable effort regarding surgical procedure and infrastructure. However, it is still at least a two-stage procedure, and with even more procedures in infected cases. Future efforts should be made to advance the technique into a one-stage procedure, while still ending with good results. At the same time, this would reduce the risks for the patients and increase the rate of application. To the knowledge of the authors, there are research groups that are aiming to solve this problem. Newly invented resorbable scaffolds combined with artificial membranes could provide such a solution. Such materials have to be biocompatible, biodegradable, and support osteogenesis while providing osteoconductivity and osteoinductivity (101). However,

further investigations are necessary to develop a single-stage surgery for critical-size defects and establish it in the clinical daily practice.

6. References

1. Verkehrsunfälle Zeitreihen 2020 [document on the internet], Statistisches Bundesamt (Destatis) (cited 12.04.2021). Verfügbar unter: https://www.destatis.de/DE/Themen/Gesellschaft-Umwelt/Verkehrsunfaelle/Publikationen/Downloads-Verkehrsunfaelle/verkehrsunfaelle-zeitreihen-pdf-5462403.pdf?__blob=publicationFile.

2. Keating JF, Simpson AH, Robinson CM. The management of fractures with bone loss. J Bone Joint Surg Br. 2005 Feb;87(2):142-50. doi: 10.1302/0301-620x.87b2.15874. PMID: 15736731.

3. Rockwood, Charles A., David P. Green, and Robert W. Bucholz. Rockwood and Green's Fractures in Adults. 6th ed. / editors, Robert W. Bucholz, James D. Heckman, Charles M. Court-Brown ; associate editors, Kenneth J. Koval, Paul Tornetta III, Michael A. Wirth. Philadelphia: Lippincott Williams & Wilkins, 2006. Print.

4. Sanders DW, Bhandari M, Guyatt G, Heels-Ansdell D, Schemitsch EH, Swiontkowski M, Tornetta P 3rd, Walter S; SPRINT Investigators. Critical-sized defect in the tibia: is it critical? Results from the SPRINT trial. J Orthop Trauma. 2014 Nov;28(11):632-5. doi: 10.1097/BOT.0000000000000194. PMID: 25233157.

5. Sato K, Watanabe Y, Harada N, Abe S, Matsushita T, Yamanaka K, Kaneko T, Sakai Y. Establishment of reproducible, critical-sized, femoral segmental bone defects in rats. Tissue Eng Part C Methods. 2014 Dec;20(12):1037-41. doi: 10.1089/ten.TEC.2013.0612. Epub 2014 Jul 10. PMID: 24738624.

6. Schmitz JP, Hollinger JO. The critical size defect as an experimental model for craniomandibulofacial nonunions. Clin Orthop Relat Res. 1986 Apr;(205):299-308. PMID: 3084153.

7. Meselhy, M.A., Elhammady, A.S. Induced Membrane Technique Using Combined Free Fibular and Iliac Graft for the Treatment of Infected Nonunion of Long Bones of the Lower Limb. SN Compr. Clin. Med. 2, 1184–1190 (2020). https://doi.org/10.1007/s42399-020-00387-w

8. Hinsche AF, Giannoudis PV, Matthews SE, Smith RM. Spontaneous healing of large femoral cortical bone defects: does genetic predisposition play a role? Acta Orthop Belg. 2003 Oct;69(5):441-6. PMID: 14648954.

9. K Keating JF, Simpson AH, Robinson CM. The management of fractures with bone loss. J Bone Joint Surg Br. 2005 Feb;87(2):142-50. doi: 10.1302/0301-620x.87b2.15874. PMID: 15736731.

10. Schemitsch EH. Size Matters: Defining Critical in Bone Defect Size! J Orthop Trauma. 2017 Oct;31 Suppl 5:S20-S22. doi: 10.1097/BOT.0000000000000978. PMID: 28938386.

11. Giannoudis PV, Einhorn TA, Marsh D. Fracture healing: the diamond concept. Injury. 2007 Sep;38 Suppl 4:S3-6. doi: 10.1016/s0020-1383(08)70003-2. PMID: 18224731.

12. Marsell R, Einhorn TA. The biology of fracture healing. Injury. 2011 Jun;42(6):551-5. doi: 10.1016/j.injury.2011.03.031. Epub 2011 Apr 13. PMID: 21489527; PMCID: PMC3105171.

13. Papachristou DJ, Georgopoulos S, Giannoudis PV, Panagiotopoulos E. Insights into the Cellular and Molecular Mechanisms That Govern the Fracture-Healing Process: A Narrative Review. J Clin Med. 2021 Aug 12;10(16):3554. doi: 10.3390/jcm10163554. PMID: 34441849; PMCID: PMC8397080.

14. Schmidt-Bleek K, Schell H, Schulz N, Hoff P, Perka C, Buttgereit F, Volk HD, Lienau J, Duda GN. Inflammatory phase of bone healing initiates the regenerative healing cascade. Cell Tissue Res. 2012 Mar;347(3):567-73. doi: 10.1007/s00441-011-1205-7. Epub 2011 Jul 26. PMID: 21789579.

15. Hankenson KD, Dishowitz M, Gray C, Schenker M. Angiogenesis in bone regeneration. Injury. 2011 Jun;42(6):556-61. doi: 10.1016/j.injury.2011.03.035. Epub 2011 Apr 12. PMID: 21489534; PMCID: PMC3105195.

16. Willie BM, Petersen A, Schmidt-Bleek K, Cipitria A, Mehta M, Strube P, Lienau J, Wildemann B, Fratzl P, Duda G. Designing biomimetic scaffolds for bone regeneration: why aim for a copy of mature tissue properties if nature uses a different approach? Soft Matter 2010; 6(20):4976. doi: 10.1039/c0sm00262c.

17. Jacobsen KA, Al-Aql ZS, Wan C, Fitch JL, Stapleton SN, Mason ZD, Cole RM, Gilbert SR, Clemens TL, Morgan EF, Einhorn TA, Gerstenfeld LC. Bone formation during distraction osteogenesis is dependent on both VEGFR1 and VEGFR2 signaling. J Bone Miner Res. 2008 May;23(5):596-609. doi: 10.1359/jbmr.080103. PMID: 18433297; PMCID: PMC2674537.

18. Schmidmaier G, Moghaddam A. Pseudarthrosen langer Röhrenknochen [Long Bone Nonunion]. Z Orthop Unfall. 2015 Dec;153(6):659-74; quiz 675-6. German. doi: 10.1055/s-0035-1558259. Epub 2015 Dec 15. PMID: 26670151.

19. Schlundt C, Bucher CH, Tsitsilonis S, Schell H, Duda GN, Schmidt-Bleek K. Clinical and Research Approaches to Treat Non-union Fracture. Curr Osteoporos Rep. 2018 Apr;16(2):155-168. doi: 10.1007/s11914-018-0432-1. PMID: 29536393.

20. Frölke JP, Patka P. Definition and classification of fracture non-unions. Injury. 2007 May;38 Suppl 2:S19-22. doi: 10.1016/s0020-1383(07)80005-2. Erratum in: Injury. 2007 Oct;38(10):1224. PMID: 17920413.

21. Märdian S, Giesecke M, Haschke F, Tsitsilonis S, Wildemann B, Schwabe P. Treatment of Tibial Non-Unions - State of the Art and Future Implications. Acta Chir Orthop Traumatol Cech. 2016;83(6):367-374. English. PMID: 28026731.

22. Giannoudis PV, Einhorn TA, Schmidmaier G, Marsh D. The diamond concept--open questions. Injury. 2008 Sep;39 Suppl 2:S5-8. doi: 10.1016/S0020-1383(08)70010-X. PMID: 18804574.

23. Weber B. G. Čech Oldřich & Konstam P. G. (1976). Pseudarthrosis : pathophysiology biomechanics therapy results. Hans Huber.

24. Epari DR, Kassi JP, Schell H, Duda GN. Timely fracture-healing requires optimization of axial fixation stability. J Bone Joint Surg Am. 2007 Jul;89(7):1575-85. doi: 10.2106/JBJS.F.00247. PMID: 17606797.

25. Gómez-Barrena E, Rosset P, Lozano D, Stanovici J, Ermthaller C, Gerbhard F. Bone fracture healing: cell therapy in delayed unions and nonunions. Bone. 2015 Jan;70:93-101. doi: 10.1016/j.bone.2014.07.033. Epub 2014 Aug 2. PMID: 25093266.

26. GOETHE, J. W. The metamorphosis of plants. Introduction and photography by G. L. Miller. MIT Press, Cambridge, Massachusetts, & London: 2009. Pp xxxi, 123; illustrated. Price US$ 21.95, UK£ 16.95. ISBN 978-0-262-01309-3 (hardback).

27. Jeyaraman M, Muthu S, Gangadaran P, Ranjan R, Jeyaraman N, Prajwal GS, Mishra PC, Rajendran RL, Ahn BC. Osteogenic and Chondrogenic Potential of Periosteum-Derived Mesenchymal Stromal Cells: Do They Hold the Key to the Future? Pharmaceuticals (Basel). 2021 Nov 8;14(11):1133. doi: 10.3390/ph14111133. PMID: 34832915; PMCID: PMC8618036.

28. Dwek JR. The periosteum: what is it, where is it, and what mimics it in its absence? Skeletal Radiol. 2010 Apr;39(4):319-23. doi: 10.1007/s00256-009-0849-9. PMID: 20049593; PMCID: PMC2826636.
29. Li C, Fennessy P. The periosteum: a simple tissue with many faces, with special reference to the antler-lineage periostea. Biol Direct. 2021 Oct 18;16(1):17. doi: 10.1186/s13062-021-00310-w. PMID: 34663443; PMCID: PMC8522104.
30. Aaron JE. Periosteal Sharpey's fibers: a novel bone matrix regulatory system? Front Endocrinol (Lausanne). 2012 Aug 9;3:98. doi: 10.3389/fendo.2012.00098. PMID: 22908007; PMCID: PMC3414712.
31. Bragdon BC, Bahney CS. Origin of Reparative Stem Cells in Fracture Healing. Curr Osteoporos Rep. 2018 Aug;16(4):490-503. doi: 10.1007/s11914-018-0458-4. PMID: 29959723; PMCID: PMC6041151.
32. Nawar K, Eliya Y, Burrow S, Peterson D, Ayeni O, de Sa D. Operative Versus Non-operative Management of Mid-diaphyseal Clavicle Fractures in the Skeletally Immature Population: A Systematic Review and Meta-analysis. Curr Rev Musculoskelet Med. 2020 Feb;13(1):38-49. doi: 10.1007/s12178-020-09604-4. PMID: 31970646; PMCID: PMC7083995.
33. Matsushima S, Isogai N, Jacquet R, Lowder E, Tokui T, Landis WJ. The nature and role of periosteum in bone and cartilage regeneration. Cells Tissues Organs. 2011;194(2-4):320-5. doi: 10.1159/000324642. Epub 2011 May 20. PMID: 21597269; PMCID: PMC3178095.
34. Clark D, Nakamura M, Miclau T, Marcucio R. Effects of Aging on Fracture Healing. Curr Osteoporos Rep. 2017 Dec;15(6):601-608. doi: 10.1007/s11914-017-0413-9. PMID: 29143915; PMCID: PMC6517062.
35. Neagu TP, Ţigliş M, Cocoloş I, Jecan CR. The relationship between periosteum and fracture healing. Rom J Morphol Embryol. 2016;57(4):1215-1220. PMID: 28174786.
36. Debnath S, Yallowitz AR, McCormick J, Lalani S, Zhang T, Xu R, Li N, Liu Y, Yang YS, Eiseman M, Shim JH, Hameed M, Healey JH, Bostrom MP, Landau DA, Greenblatt MB. Discovery of a periosteal stem cell mediating intramembranous bone formation. Nature. 2018 Oct;562(7725):133-139. doi: 10.1038/s41586-018-0554-8. Epub 2018 Sep 24. PMID: 30250253; PMCID: PMC6193396.
37. Ito R, Matsumiya T, Kon T, Narita N, Kubota K, Sakaki H, Ozaki T, Imaizumi T, Kobayashi W, Kimura H. Periosteum-derived cells respond to mechanical stretch and

activate Wnt and BMP signaling pathways. Biomed Res. 2014;35(1):69-79. doi: 10.2220/biomedres.35.69. PMID: 24573203.

38. Chen D, Zhao M, Mundy GR. Bone morphogenetic proteins. Growth Factors. 2004 Dec;22(4):233-41. doi: 10.1080/08977190412331279890. PMID: 15621726.

39. Zhou S. TGF-β regulates β-catenin signaling and osteoblast differentiation in human mesenchymal stem cells. J Cell Biochem. 2011 Jun;112(6):1651-60. doi: 10.1002/jcb.23079. PMID: 21344492; PMCID: PMC3079785.

40. Wolff J. The Law of Bone Remodeling. Berlin Heidelberg New York: Springer; 1986. (translation of the German 1892 edition, Das Gesetz der Transformation der Knochen.). doi: 10.1007/978-3-642-71031-5.

41. Albrektsson T, Johansson C. Osteoinduction, osteoconduction and osseointegration. Eur Spine J. 2001 Oct;10 Suppl 2(Suppl 2):S96-101. doi: 10.1007/s005860100282. PMID: 11716023; PMCID: PMC3611551.

42. Marais, Leonard & Ferreira, Nando & Aldous, Colleen & Roux, Theo. (2014). The management of chronic osteomyelitis: Part I - Diagnostic work-up and surgical principles. South African Orthopaedic Journal. 13. 42.

43. Rodríguez-Merchán EC. A Review of Recent Developments in the Molecular Mechanisms of Bone Healing. Int J Mol Sci. 2021 Jan 14;22(2):767. doi: 10.3390/ijms22020767. PMID: 33466612; PMCID: PMC7828700.

44. Cuthbert RJ, Jones E, Sanjurjo-Rodríguez C, Lotfy A, Ganguly P, Churchman SM, Castana P, Tan HB, McGonagle D, Papadimitriou E, Giannoudis PV. Regulation of Angiogenesis Discriminates Tissue Resident MSCs from Effective and Defective Osteogenic Environments. J Clin Med. 2020 May 28;9(6):1628. doi: 10.3390/jcm9061628. PMID: 32481579; PMCID: PMC7355658.

45. Strokov VN. O tekhnike udlineniia nizhnikh konechnosteĭ pri ikh ukorocheniiakh i vozmeshchenie kostnykh defektov po metodu G. A. Ilizarova [Technic of leg elongation after shortening, and compensation for bone defects by G. A. Ilizarov's method]. Ortop Travmatol Protez. 1971 Nov;32(11):37-42. Russian. PMID: 5141239.

46. Gubin AV, Borzunov DY, Marchenkova LO, Malkova TA, Smirnova IL. Contribution of G.A. Ilizarov to bone reconstruction: historical achievements and state of the art. Strategies Trauma Limb Reconstr. 2016 Nov;11(3):145-152. doi: 10.1007/s11751-016-0261-7. Epub 2016 Jul 18. PMID: 27432154; PMCID: PMC5069200.

47. Spiegelberg B, Parratt T, Dheerendra SK, Khan WS, Jennings R, Marsh DR. Ilizarov principles of deformity correction. Ann R Coll Surg Engl. 2010 Mar;92(2):101-5. doi: 10.1308/003588410X12518836439326. PMID: 20353638; PMCID: PMC3025247.
48. Gubin AV, Borzunov DY, Malkova TA. The Ilizarov paradigm: thirty years with the Ilizarov method, current concerns and future research. Int Orthop. 2013 Aug;37(8):1533-9. doi: 10.1007/s00264-013-1935-0. Epub 2013 May 28. PMID: 23712212; PMCID: PMC3728395.
49. Szelerski Ł, Pajchert Kozłowska A, Żarek S, Górski R, Mochocki K, Dejnek M, Urbański W, Reichert P, Morasiewicz P. A new criterion for assessing Ilizarov treatment outcomes in nonunion of the tibia. Arch Orthop Trauma Surg. 2021 May;141(5):879-889. doi: 10.1007/s00402-020-03571-8. Epub 2020 Aug 10. PMID: 32778920; PMCID: PMC8049889.
50. Borzunov DY, Kolchin SN, Malkova TA. Role of the Ilizarov non-free bone plasty in the management of long bone defects and nonunion: Problems solved and unsolved. World J Orthop. 2020 Jun 18;11(6):304-318. doi: 10.5312/wjo.v11.i6.304. PMID: 32572367; PMCID: PMC7298454.
51. Aktuglu K, Erol K, Vahabi A. Ilizarov bone transport and treatment of critical-sized tibial bone defects: a narrative review. J Orthop Traumatol. 2019 Apr 16;20(1):22. doi: 10.1186/s10195-019-0527-1. PMID: 30993461; PMCID: PMC6468024.
52. Kähler Olesen U. „Plate-assisted segmental bone transport“ mit Verlängerungsnagel und Platte : Neue Technik zur Behandlung von Knochendefekten in Tibia und Femur [Plate-assisted segmental bone transport with a lengthening nail and a plate : A new technique for treatment of tibial and femoral bone defects]. Unfallchirurg. 2018 Nov;121(11):874-883. German. doi: 10.1007/s00113-018-0546-z. PMID: 30242443.
53. Mathieu L, Durand M, Collombet JM, de Rousiers A, de l'Escalopier N, Masquelet AC. Induced membrane technique: a critical literature analysis and proposal for a failure classification scheme. Eur J Trauma Emerg Surg. 2021 Oct;47(5):1373-1380. doi: 10.1007/s00068-020-01540-9. Epub 2020 Nov 23. PMID: 33226484.
54. Bezstarosti H, Metsemakers WJ, van Lieshout EMM, Voskamp LW, Kortram K, McNally MA, Marais LC, Verhofstad MHJ. Management of critical-sized bone defects in the treatment of fracture-related infection: a systematic review and pooled analysis. Arch

Orthop Trauma Surg. 2021 Jul;141(7):1215-1230. doi: 10.1007/s00402-020-03525-0. Epub 2020 Aug 29. PMID: 32860565; PMCID: PMC8215045.

55. Barakat AH, Sayani J, O'Dowd-Booth C, Guryel E. Lengthening Nails for Distraction Osteogenesis: A Review of Current Practice and Presentation of Extended Indications. Strategies Trauma Limb Reconstr. 2020 Jan-Apr;15(1):54-61. doi: 10.5005/jp-journals-10080-1451. PMID: 33363643; PMCID: PMC7744668.

56. Olesen UK, Nygaard T, Prince DE, Gardner MP, Singh UM, McNally MA, Green CJ, Herzenberg JE. Plate-assisted Bone Segment Transport With Motorized Lengthening Nails and Locking Plates: A Technique to Treat Femoral and Tibial Bone Defects. J Am Acad Orthop Surg Glob Res Rev. 2019 Aug 12;3(8):e064. doi: 10.5435/JAAOSGlobal-D-19-00064. PMID: 31592010; PMCID: PMC6754216.

57. Gardner MP, Beason AM. Plate-Assisted Bone Segment Transport Versus Precice Bone Transport Nail. J Orthop Trauma. 2021 Oct 1;35(Suppl 4):S19-S24. doi: 10.1097/BOT.0000000000002123. PMID: 34533482.

58. Rizzo M, Moran SL. Vascularized bone grafts and their applications in the treatment of carpal pathology. Semin Plast Surg. 2008 Aug;22(3):213-27. doi: 10.1055/s-2008-1081404. PMID: 20567715; PMCID: PMC2884887.

59. Vidal L, Kampleitner C, Brennan MÁ, Hoornaert A, Layrolle P. Reconstruction of Large Skeletal Defects: Current Clinical Therapeutic Strategies and Future Directions Using 3D Printing. Front Bioeng Biotechnol. 2020 Feb 12;8:61. doi: 10.3389/fbioe.2020.00061. PMID: 32117940; PMCID: PMC7029716.

60. De Santis G, Pinelli M, Starnoni M. Extended and unusual indications in jaw reconstruction with the fibula flap: An overview based on our 30-year experience. Ann Med Surg (Lond). 2021 Jan 5;62:37-42. doi: 10.1016/j.amsu.2020.12.049. PMID: 33489114; PMCID: PMC7806501.

61. Manfrini M, Innocenti M, Ceruso M, Mercuri M. Original biological reconstruction of the hip in a 4-year-old girl. Lancet. 2003 Jan 11;361(9352):140-2. doi: 10.1016/S0140-6736(03)12192-7. PMID: 12531584.

62. Baldwin P, Li DJ, Auston DA, Mir HS, Yoon RS, Koval KJ. Autograft, Allograft, and Bone Graft Substitutes: Clinical Evidence and Indications for Use in the Setting of Orthopaedic Trauma Surgery. J Orthop Trauma. 2019 Apr;33(4):203-213. doi: 10.1097/BOT.0000000000001420. PMID: 30633080.

63. Keating JF, McQueen MM. Substitutes for autologous bone graft in orthopaedic trauma. J Bone Joint Surg Br. 2001 Jan;83(1):3-8. doi: 10.1302/0301-620x.83b1.11952. Erratum in: J Bone Joint Surg Br 2001 Jul;83(5):777. PMID: 11245534.

64. Muscolo DL, Ayerza MA, Aponte-Tinao L, Ranalletta M, Abalo E. Intercalary femur and tibia segmental allografts provide an acceptable alternative in reconstructing tumor resections. Clin Orthop Relat Res. 2004 Sep;(426):97-102. doi: 10.1097/01.blo.0000141652.93178.10. PMID: 15346058.

65. Christou C, Oliver RA, Yu Y, Walsh WR. The Masquelet technique for membrane induction and the healing of ovine critical sized segmental defects. PLoS One. 2014 Dec 2;9(12):e114122. doi: 10.1371/journal.pone.0114122. PMID: 25461340; PMCID: PMC4252083.

66. Dimitriou R, Jones E, McGonagle D, Giannoudis PV. Bone regeneration: current concepts and future directions. BMC Med. 2011 May 31;9:66. doi: 10.1186/1741-7015-9-66. PMID: 21627784; PMCID: PMC3123714.

67. Masquelet AC, Fitoussi F, Begue T, Muller GP. Reconstruction des os longs par membrane induite et autogreffe spongieuse [Reconstruction of the long bones by the induced membrane and spongy autograft]. Ann Chir Plast Esthet. 2000 Jun;45(3):346-53. French. PMID: 10929461.

68. Andrzejowski P, Masquelet A, Giannoudis PV. Induced Membrane Technique (Masquelet) for Bone Defects in the Distal Tibia, Foot, and Ankle: Systematic Review, Case Presentations, Tips, and Techniques. Foot Ankle Clin. 2020 Dec;25(4):537-586. doi: 10.1016/j.fcl.2020.08.013. PMID: 33543716.

69. Pelissier P, Masquelet AC, Bareille R, Pelissier SM, Amedee J. Induced membranes secrete growth factors including vascular and osteoinductive factors and could stimulate bone regeneration. J Orthop Res. 2004 Jan;22(1):73-9. doi: 10.1016/S0736-0266(03)00165-7. PMID: 14656662.

70. Masquelet A, Kanakaris NK, Obert L, Stafford P, Giannoudis PV. Bone Repair Using the Masquelet Technique. J Bone Joint Surg Am. 2019 Jun 5;101(11):1024-1036. doi: 10.2106/JBJS.18.00842. PMID: 31169581.

71. Gindraux F, Loisel F, Bourgeois M, Oudina K, Melin M, de Billy B, Sergent P, Leclerc G, Petite H, Auber F, Obert L, Pluvy I. Induced membrane maintains its osteogenic properties even when the second stage of Masquelet's technique is performed later. Eur J Trauma Emerg Surg. 2020 Apr;46(2):301-312. doi: 10.1007/s00068-019-

01184-4. Epub 2019 Jul 18. Erratum in: Eur J Trauma Emerg Surg. 2019 Oct 30;: PMID: 31321472.

72. Niikura T, Jimbo N, Komatsu M, Oe K, Fukui T, Matsumoto T, Hayashi S, Matsushita T, Sakai Y, Itoh T, Kuroda R. Histological analysis of induced membranes in patients whose bone defects were treated with the Masquelet technique to identify factors affecting the vascularity of induced membranes. J Orthop Surg Res. 2021 Apr 13;16(1):248. doi: 10.1186/s13018-021-02404-7. PMID: 33849590; PMCID: PMC8042897.

73. Masquelet AC. Induced Membrane Technique: Pearls and Pitfalls. J Orthop Trauma. 2017 Oct;31 Suppl 5:S36-S38. doi: 10.1097/BOT.0000000000000979. PMID: 28938390.

74. Masquelet AC. The induced membrane technique. Orthop Traumatol Surg Res. 2020 Sep;106(5):785-787. doi: 10.1016/j.otsr.2020.06.001. Epub 2020 Aug 8. PMID: 32782174.

75. Choufani C, Demoures T, de l'Escalopier N, Chapon MP, Barbier O, Mathieu L. Application of the Masquelet technique in austere environments: experience from a French forward surgical unit deployed in Chad. Eur J Trauma Emerg Surg. 2022 Feb;48(1):593-599. doi: 10.1007/s00068-020-01471-5. Epub 2020 Aug 28. PMID: 32857239.

76. Mathieu L, Tossou-Odjo L, de l'Escalopier N, Demoures T, Baus A, Brachet M, Masquelet AC. Induced membrane technique with sequential internal fixation: use of a reinforced spacer for reconstruction of infected bone defects. Int Orthop. 2020 Sep;44(9):1647-1653. doi: 10.1007/s00264-020-04735-2. Epub 2020 Jul 21. PMID: 32696330.

77. Metsemakers WJ, Morgenstern M, Senneville E, Borens O, Govaert GAM, Onsea J, Depypere M, Richards RG, Trampuz A, Verhofstad MHJ, Kates SL, Raschke M, McNally MA, Obremskey WT; Fracture-Related Infection (FRI) group. General treatment principles for fracture-related infection: recommendations from an international expert group. Arch Orthop Trauma Surg. 2020 Aug;140(8):1013-1027. doi: 10.1007/s00402-019-03287-4. Epub 2019 Oct 29. PMID: 31659475; PMCID: PMC7351827.

78. Karger C, Kishi T, Schneider L, Fitoussi F, Masquelet AC; French Society of Orthopaedic Surgery and Traumatology (SoFCOT). Treatment of posttraumatic bone

defects by the induced membrane technique. Orthop Traumatol Surg Res. 2012 Feb;98(1):97-102. doi: 10.1016/j.otsr.2011.11.001. Epub 2012 Jan 12. PMID: 22244249.
79. ICD-10-CM Diagnosis Code M89.70 Major osseous defect, unspecified site (document on the internet) ICD10Data.com 2022 (cited 28.02.2022). Verfügbar unter: https://www.icd10data.com/ICD10CM/Codes/M00-M99/M86-M90/M89-/M89.70.
80. Provided by the non-profit organization “Was hab’ ich?” gemeinnützige GmbH on behalf of the Federal Ministry of Health (BMG) (cited 01.03.2022). Verfügbar unter: https://gesund.bund.de/en/icd-code-search/m84.
81. ICD.10 code: M84 Disorders of continuity of bone [document on the internet], Statistisches Bundesamt (Destatis) (cited 01.03.2022). Verfügbar unter: https://gesund.bund.de/en/icd-code-search/m84-1.
82. Tiefgegliederte Diagnosedaten der Krankenhauspatientinnen und -patienten 2019 [document on the internet], Statistisches Bundesamt (Destatis) (cited 28.02.2022). Verfügbar unter: https://www.destatis.de/DE/Themen/Gesellschaft-Umwelt/Gesundheit/Krankenhaeuser/Publikationen/Downloads-Krankenhaeuser/tiefgegliederte-diagnosedaten-5231301197015.html.
83. Tiefgegliederte Diagnosedaten der Krankenhauspatientinnen und -patienten 2018 [document on the internet], Statistisches Bundesamt (Destatis) (cited 28.02.2022). Verfügbar unter: https://www.statistischebibliothek.de/mir/receive/DEHeft_mods_00131401.
84. Tiefgegliederte Diagnosedaten der Krankenhauspatientinnen und -patienten 2017 [document on the internet], Statistisches Bundesamt (Destatis) (cited 28.02.2022). Verfügbar unter: https://www.statistischebibliothek.de/mir/receive/DEHeft_mods_00131400.
85. Bustin SA, Benes V, Garson JA, Hellemans J, Huggett J, Kubista M, Mueller R, Nolan T, Pfaffl MW, Shipley GL, Vandesompele J, Wittwer CT. The MIQE guidelines: minimum information for publication of quantitative real-time PCR experiments. Clin Chem. 2009 Apr;55(4):611-22. doi: 10.1373/clinchem.2008.112797. Epub 2009 Feb 26. PMID: 19246619.
86. Adams G. A beginner’s guide to RT-PCR, qPCR and RT-qPCR. The Biochemist (Lond) 22 June 2020; 42(3):48–53. doi: 10.1042/BIO20200034.

87. Dheda K, Huggett JF, Bustin SA, Johnson MA, Rook G, Zumla A. Validation of housekeeping genes for normalizing RNA expression in real-time PCR. Biotechniques. 2004 Jul;37(1):112-4, 116, 118-9. doi: 10.2144/04371RR03. PMID: 15283208.

88. Applied Biosystems 11.2010. TaqMan® Gene Expression Assays Protocol (PN 4333458N) [document on the internet] (cited 29.11.2021). Verfügbar unter: https://tools.thermofisher.com/content/sfs/manuals/cms_041280.pdf.

89. König D, Oesser S, Scharla S, Zdzieblik D, Gollhofer A. Specific Collagen Peptides Improve Bone Mineral Density and Bone Markers in Postmenopausal Women-A Randomized Controlled Study. Nutrients. 2018 Jan 16;10(1):97. doi: 10.3390/nu10010097. PMID: 29337906; PMCID: PMC5793325.

90. Ibrahim MM, Chen L, Bond JE, Medina MA, Ren L, Kokosis G, Selim AM, Levinson H. Myofibroblasts contribute to but are not necessary for wound contraction. Lab Invest. 2015 Dec;95(12):1429-38. doi: 10.1038/labinvest.2015.116. Epub 2015 Sep 14. PMID: 26367489; PMCID: PMC4861064.

91. Chitturi RT, Balasubramaniam AM, Parameswar RA, Kesavan G, Haris KT, Mohideen K. The role of myofibroblasts in wound healing, contraction and its clinical implications in cleft palate repair. J Int Oral Health. 2015 Mar;7(3):75-80. PMID: 25878485; PMCID: PMC4385733.

92. Alarcon-Martinez L, Yilmaz-Ozcan S, Yemisci M, Schallek J, Kılıç K, Can A, Di Polo A, Dalkara T. Capillary pericytes express α-smooth muscle actin, which requires prevention of filamentous-actin depolymerization for detection. Elife. 2018 Mar 21;7:e34861. doi: 10.7554/eLife.34861. PMID: 29561727; PMCID: PMC5862523.

93. Owston HE, Moisley KM, Tronci G, Russell SJ, Giannoudis PV, Jones E. Induced Periosteum-Mimicking Membrane with Cell Barrier and Multipotential Stromal Cell (MSC) Homing Functionalities. Int J Mol Sci. 2020 Jul 23;21(15):5233. doi: 10.3390/ijms21155233. PMID: 32718036; PMCID: PMC7432450.

94. Arnsdorf EJ, Jones LM, Carter DR, Jacobs CR. The periosteum as a cellular source for functional tissue engineering. Tissue Eng Part A. 2009 Sep;15(9):2637-42. doi: 10.1089/ten.TEA.2008.0244. PMID: 19207046; PMCID: PMC2792114.

95. Xie J, Liu D, Wang H, Long H, Zhu Y, Hu Y, Zeng M. Effects of topical mechanical stability on the formation of Masquelet membrane in a rabbit radial defect model. Sci Rep. 2020 Nov 3;10(1):18939. doi: 10.1038/s41598-020-76112-3. PMID: 33144701; PMCID: PMC7609590.

96. Woodfin A, Voisin MB, Nourshargh S. PECAM-1: a multi-functional molecule in inflammation and vascular biology. Arterioscler Thromb Vasc Biol. 2007 Dec;27(12):2514-23. doi: 10.1161/ATVBAHA.107.151456. Epub 2007 Sep 13. PMID: 17872453.

97. Crisera CA, Maldonado TS, Kadison AS, Li M, Alkasab SL, Longaker MT, Gittes GK. Transforming growth factor-beta 1 in the developing mouse pancreas: a potential regulator of exocrine differentiation. Differentiation. 2000 May;65(5):255-9. doi: 10.1046/j.1432-0436.2000.6550255.x. PMID: 10929204.

98. Susol E, Rands AL, Herrick A, McHugh N, Barrett JH, Ollier WE, Worthington J. Association of markers for TGFbeta3, TGFbeta2 and TIMP1 with systemic sclerosis. Rheumatology (Oxford). 2000 Dec;39(12):1332-6. doi: 10.1093/rheumatology/39.12.1332. PMID: 11136875.

99. Verboket RD, Leiblein M, Janko M, Schaible A, Brune JC, Schröder K, Heilani M, Fremdling C, Busche Y, Irrle T, Marzi I, Nau C, Henrich D. From two stages to one: acceleration of the induced membrane (Masquelet) technique using human acellular dermis for the treatment of non-infectious large bone defects. Eur J Trauma Emerg Surg. 2020 Apr;46(2):317-327. doi: 10.1007/s00068-019-01296-x. Epub 2020 Jan 13. PMID: 31932852; PMCID: PMC7113234.

100. Ganguly P, Jones E, Panagiotopoulou V, Jha A, Blanchy M, Antimisiaris S, Anton M, Dhuiège B, Marotta M, Marjanovic N, Panagiotopoulos E, Giannoudis PV. Electrospun and 3D printed polymeric materials for one-stage critical-size long bone defect regeneration inspired by the Masquelet technique: Recent Advances. Injury. 2022 Oct;53 Suppl 2:S2-S12. doi: 10.1016/j.injury.2022.02.036. Epub 2022 Feb 16. PMID: 35305805.

101. Pobloth AM, Schell H, Petersen A, Beierlein K, Kleber C, Schmidt-Bleek K, Duda GN. Tubular open-porous β-tricalcium phosphate polycaprolactone scaffolds as guiding structure for segmental bone defect regeneration in a novel sheep model. J Tissue Eng Regen Med. 2018 Apr;12(4):897-911. doi: 10.1002/term.2446. Epub 2017 Jun 29. PMID: 28485078.

102. Leiblein M, Koch E, Winkenbach A, Schaible A, Nau C, Büchner H, Schröder K, Marzi I, Henrich D. Size matters: Effect of granule size of the bone graft substitute (Herafill®) on bone healing using Masquelet's induced membrane in a critical size defect model in the rat's femur. J Biomed Mater Res B Appl Biomater. 2020 May;108(4):1469-1482. doi: 10.1002/jbm.b.34495. Epub 2019 Nov 13. PMID: 31721435.

103. Giannoudis PV, Tosounidis TH. Acute and chronic infection: Is there a gold standard for management of the wound and bone defect? OTA Int. 2020 Mar 23;3(1):e068. doi: 10.1097/OI9.0000000000000068. PMID: 33937688; PMCID: PMC8081461.
104. Giannoudis PV, Krettek C, Lowenberg DW, Tosounidis T, Borrelli J Jr. Fracture Healing Adjuncts-The World's Perspective on What Works. J Orthop Trauma. 2018 Mar;32 Suppl 1:S43-S47. doi: 10.1097/BOT.0000000000001127. PMID: 29461403.
105. Cuthbert RJ, Churchman SM, Tan HB, McGonagle D, Jones E, Giannoudis PV. Induced periosteum a complex cellular scaffold for the treatment of large bone defects. Bone. 2013 Dec;57(2):484-92. doi: 10.1016/j.bone.2013.08.009. Epub 2013 Aug 15. PMID: 23954755.

7. Eidesstattliche Versicherung

„Ich, Anselm Rommel, versichere an Eides statt durch meine eigenhändige Unterschrift, dass ich die vorgelegte Dissertation mit dem Thema: „The Importance of the periosteum and the induced membrane for bone healing“ / „Die Bedeutung des Periosts und der induzierten Membran für die Knochenheilung“ selbstständig und ohne nicht offengelegte Hilfe Dritter verfasst und keine anderen als die angegebenen Quellen und Hilfsmittel genutzt habe.

Alle Stellen, die wörtlich oder dem Sinne nach auf Publikationen oder Vorträgen anderer Autoren/innen beruhen, sind als solche in korrekter Zitierung kenntlich gemacht. Die Abschnitte zu Methodik (insbesondere praktische Arbeiten, Laborbestimmungen, statistische Aufarbeitung) und Resultaten (insbesondere Abbildungen, Graphiken und Tabellen) werden von mir verantwortet.
Ich versichere ferner, dass ich die in Zusammenarbeit mit anderen Personen generierten Daten, Datenauswertungen und Schlussfolgerungen korrekt gekennzeichnet und meinen eigenen Beitrag sowie die Beiträge anderer Personen korrekt kenntlich gemacht habe (siehe Anteilserklärung). Texte oder Textteile, die gemeinsam mit anderen erstellt oder verwendet wurden, habe ich korrekt kenntlich gemacht.

Meine Anteile an etwaigen Publikationen zu dieser Dissertation entsprechen denen, die in der untenstehenden gemeinsamen Erklärung mit dem/der Erstbetreuer/in, angegeben sind. Für sämtliche im Rahmen der Dissertation entstandenen Publikationen wurden die Richtlinien des ICMJE (International Committee of Medical Journal Editors; www.icmje.og) zur Autorenschaft eingehalten. Ich erkläre ferner, dass ich mich zur Einhaltung der Satzung der Charité – Universitätsmedizin Berlin zur Sicherung Guter Wissenschaftlicher Praxis verpflichte.

Weiterhin versichere ich, dass ich diese Dissertation weder in gleicher noch in ähnlicher Form bereits an einer anderen Fakultät eingereicht habe.

Die Bedeutung dieser eidesstattlichen Versicherung und die strafrechtlichen Folgen einer unwahren eidesstattlichen Versicherung (§§156, 161 des Strafgesetzbuches) sind mir bekannt und bewusst.“

13.03.2023 _____ _____

Datum Unterschrift

8. Curriculum Vitae

Mein Lebenslauf wird aus datenschutzrechtlichen Gründen in der elektronischen Version meiner Arbeit nicht veröffentlicht.

9. Acknowledgements

An dieser Stelle möchte ich meinen besonderen Dank an die Personen ausdrücken, durch deren Mithilfe die Arbeit zustande kommen konnte:

Zunächst bei meinem Doktorvater Herr PD Dr. med. Sven Märdian, Oberarzt des Centrums für Muskuloskelettale Chirurgie der Charité – Universitätsmedizin Berlin am Campus Virchow-Klinikum, sowie Univ.-Prof. Dr.-Ing. Georg Duda, Direktor des Julius-Wolff-Instituts für Biomechanik und Muskuloskelettale Regeneration, für die Bereitstellung des klinischen Materials, der Ermöglichung der Durchführung der labortechnischen Untersuchungen und der Möglichkeit der Abfassung der Arbeit.

Mein besonderer Dank gilt PD Dr. rer. nat. Katharina Schmidt-Bleek, für die kontinuierliche Betreuung Förderung und Ermutigung zur wissenschaftlichen Arbeit.

Zu innigem Dank bin ich auch Gabriele Rußow verpflichtet, der ich mich freundschaftlich für ihre zahlreichen Hinweise, Hilfestellungen und Unterstützung verbunden fühle.

Danke an das ganze Team der AG-KSB für die wöchentlichen Diskussionen und Ratschläge, Christian, Radost, Raphael, Lisa, Anni, Sabine, Anke, Sevim, Heilwig. Hier hervorheben möchte ich dich Norma. Es war nicht selbstverständlich und daher weiß ich es sehr zu schätzen, dass du stets verständnisvoll und nachsichtig mir gegenüber warst und ich dich auch am Wochenende um Hilfe bitten konnte.

Mein größter Dank gilt meinen Eltern, die immer und jederzeit für mich da waren, die immer ein offenes Ohr für alle meine Belange hatten und mich in jeglicher Form absolut bedingungslos unterstützt haben. Ihr ermöglicht mir meinen Lebensweg und daher widme ich euch diese Arbeit.

10. Statistische Bescheinigung

CharitéCentrum für Human- und Gesundheitswissenschaften

Charité Campus Charité Mitte 10117 Berlin

Institut für Biometrie und klinische Epidemiologie (iBikE)

Direktor: Prof. Dr. Frank Konietschke

Postanschrift:
Charitéplatz 1 | 10117 Berlin
Besucheranschrift:
Reinhardtstr. 58 | 10117 Berlin

Tel. +49 (0)30 450 562171
frank.konietschke@charite.de
https://biometrie.charite.de/

Name, Vorname: Rommel, Anselm

Emailadresse: anselm.rommel@charite.de

Matrikelnummer: 228375

PromotionsbetreuerIn: PD Dr. Märdian

Promotionsinstitution / Klinik: Centrum für Muskuloskelettale Chirurgie
Klinik für Orthopädie und Klinik für Unfall- und Wiederherstellungschirurgie Campus Virchow Klinikum und dem Julius-Wolff-Institut
der Medizinischen Fakultät Charité - Universitätsmedizin Berlin

Bescheinigung

Hiermit bescheinige ich, dass *Herr Anselm Rommel* innerhalb der Service Unit Biometrie des Instituts für Biometrie und klinische Epidemiologie (iBikE) bei mir eine statistische Beratung zu einem Promotionsvorhaben wahrgenommen hat. Folgende Beratungstermine wurden wahrgenommen:

 Termin 1: 07.03.2023

Folgende wesentliche Ratschläge hinsichtlich einer sinnvollen Auswertung und Interpretation der Daten wurden während der Beratung erteilt:

- Eine tiefergreifende statistische Auswertung war in diesem Falle nicht angemessen. Ich unterstütze die Durchführung und bildliche Darstellung der Expression Analysis

Diese Bescheinigung garantiert nicht die richtige Umsetzung der in der Beratung gemachten

Vorschläge, die korrekte Durchführung der empfohlenen statistischen Verfahren und die richtige

Darstellung und Interpretation der Ergebnisse. Die Verantwortung hierfür obliegt allein dem Promovierenden. Das Institut für Biometrie und klinische Epidemiologie übernimmt hierfür keine Haftung.